Research Article
Cirrhosis and Liver Failure

JOURNAL
OF HEPATOLOGY

Lysophosphatidylcholines modulate immunoregulatory checkpoints in peripheral monocytes and are associated with mortality in people with acute liver failure

Authors

Francesca M. Trovato, Rabiya Zia, Florent Artru, …, Stephen R. Atkinson, Evangelos Triantafyllou, Mark J.W. McPhail

Correspondence

francesca.trovato@kcl.ac.uk (F.M. Trovato).

Graphical abstract

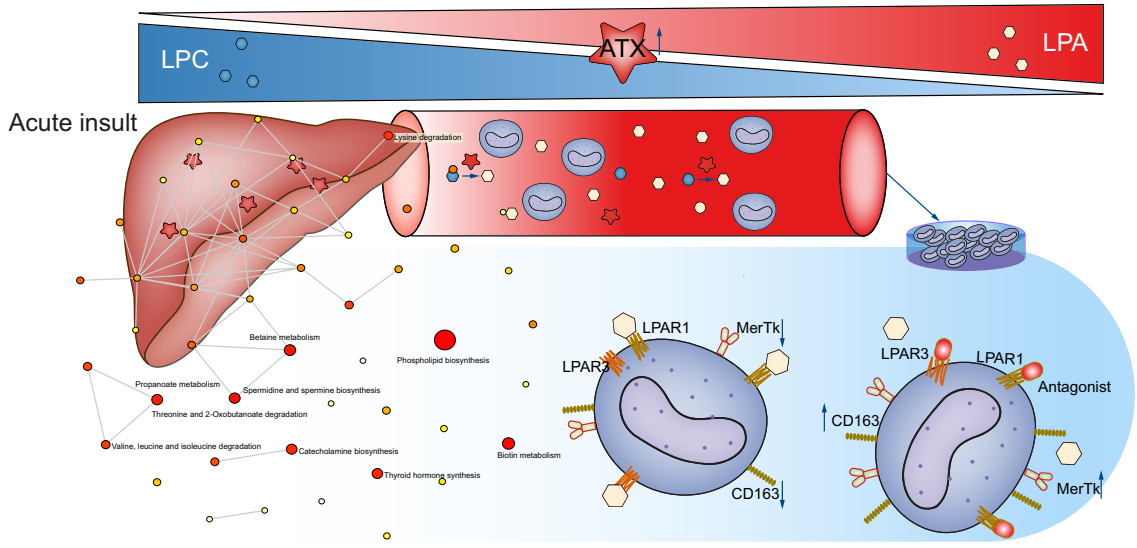

Highlights

- Plasma lysophosphatidylcholines are reduced and can be used as prognostic markers of poor outcome in ALF.
- The LPC-ATX-LPA axis appears to modulate innate immune response in ALF via MerTK and CD163 expression.
- LPAR1 and LPAR3 antagonism reverses the effects of LPA on monocyte phenotype.

Impact and implications

We identified a metabolic signature of acute liver failure (ALF) and investigated the immunometabolic role of the lysophosphatidylcholine-autotaxin-lysophosphatidylcholinic acid pathway, with the aim of finding a mechanistic explanation for monocyte behaviour and identifying possible therapeutic targets (to modulate the systemic immune response in ALF). At present, no selective immune-based therapies exist. We were able to modulate the phenotype of monocytes *in vitro* and aim to extend these findings to murine models of ALF as a next step. Future therapies may be based on metabolic modulation; thus, the role of specific lipids in this pathway require elucidation and the relative merits of autotaxin inhibition, lysophosphatidylcholinic acid receptor blockade or lipid-based therapies need to be determined. Our findings begin to bridge this knowledge gap and the methods used herein could be useful in identifying therapeutic targets as part of an experimental medicine approach.

https://doi.org/10.1016/j.jhep.2022.10.031

Research Article
Cirrhosis and Liver Failure

JOURNAL
OF HEPATOLOGY

Lysophosphatidylcholines modulate immunoregulatory checkpoints in peripheral monocytes and are associated with mortality in people with acute liver failure

Francesca M. Trovato[1,2,*], Rabiya Zia[3], Florent Artru[1,2], Salma Mujib[2], Ellen Jerome[1,2], Anna Cavazza[1,2], Muireann Coen[3,4], Ian Wilson[3], Elaine Holmes[3], Phillip Morgan[2], Arjuna Singanayagam[2,6], Christine Bernsmeier[2,7], Salvatore Napoli[2], William Bernal[2], Julia Wendon[2], Rosa Miquel[2], Krishna Menon[2], Vishal C. Patel[1,2,5], John Smith[8], Stephen R. Atkinson[3], Evangelos Triantafyllou[3], Mark J.W. McPhail[1,2]

Journal of Hepatology **2022**. vol. ■ | 1–16

Background & Aims: Acute liver failure (ALF) is a life-threatening disease characterised by high-grade inflammation and immunoparesis, which is associated with a high incidence of death from sepsis. Herein, we aimed to describe the metabolic dysregulation in ALF and determine whether systemic immune responses are modulated *via* the lysophosphatidylcholine (LPC)-autotaxin (ATX)-lysophosphatidylcholinic acid (LPA) pathway.
Methods: Ninety-six individuals with ALF, 104 with cirrhosis, 31 with sepsis and 71 healthy controls (HCs) were recruited. Pathways of interest were identified by multivariate statistical analysis of proton nuclear magnetic resonance spectroscopy and untargeted ultraperformance liquid chromatography-mass spectrometry-based lipidomics. A targeted metabolomics panel was used for validation. Peripheral blood mononuclear cells were cultured with LPA 16:0, 18:0, 18:1, and their immune checkpoint surface expression was assessed by flow cytometry. Transcript-level expression of the LPA receptor (*LPAR*) in monocytes was investigated and the effect of LPAR antagonism was also examined *in vitro*.
Results: LPC 16:0 was highly discriminant between ALF and HC. There was an increase in ATX and LPA in individuals with ALF compared to HCs and those with sepsis. LPCs 16:0, 18:0 and 18:1 were reduced in individuals with ALF and were associated with a poor prognosis. Treatment of monocytes with LPA 16:0 increased their PD-L1 expression and reduced CD155, CD163, MerTK levels, without affecting immune checkpoints on T and NK/CD56+T cells. LPAR1 and 3 antagonism in culture reversed the LPA effect on monocyte expression of MerTK and CD163. MerTK and CD163, but not *LPAR* genes, were differentially expressed and upregulated in monocytes from individuals with ALF compared to controls.
Conclusion: Reduced LPC levels are biomarkers of poor prognosis in individuals with ALF. The LPC-ATX-LPA axis appears to modulate innate immune response in ALF via LPAR1 and LPAR3. Further investigations are required to identify novel therapeutic agents targeting these receptors.

Introduction

Acute liver failure (ALF) is a rare life-threatening disease characterised by acute derangement of liver synthetic function with coagulopathy and altered levels of consciousness from hepatic encephalopathy in people without previous liver disease.[1] ALF is characterised by intense systemic inflammation and parallel impairment of innate and adaptive antimicrobial immune responses (immunoparesis), and is associated with a high incidence of death from sepsis and multiorgan failure.[2] In this context, immune cell function is often suppressed by multiple mechanisms, including inhibitory signalling *via* immune checkpoint pathways, such as programmed cell death 1 (PD-1)[3] and cytotoxic T-lymphocyte-associated protein 4 (CTLA4).[4] However, no selective immune-based therapies exist for ALF.

The association between ALF and sepsis is due to a switch of the innate immune system to a regulatory, anti-inflammatory mode during the first week of illness, as systemic inflammation subsides. Expression of MerTK (mediating the efferocytosis of apoptotic cell) and CD163 (a scavenger receptor) increases in peripheral monocytes and hepatic macrophages favour tissue repair at the expense of a higher risk of sepsis.[5,6] We recently demonstrated that PD-1 blockade restored human monocyte functionality *in vitro* while PD-1-deficient mice and anti-PD-1-treated mice with liver injury showed improved Kupffer cell bacterial clearance and protection from sepsis.[3] However,

Keywords: lysophosphatidylcholine; acute liver failure; immune checkpoint; LPAR; MerTK; CD163; RNA sequencing; Monocytes.
Received 16 March 2022; received in revised form 17 October 2022; accepted 19 October 2022; available online xxx
* Corresponding author. Address: Institute of Liver Studies, School of Immunology & Microbial Science, Kings College London, SE5 9RS Denmark Hill, London. Tel.: +4402032996280.
E-mail address: francesca.trovato@kcl.ac.uk (F.M. Trovato).
https://doi.org/10.1016/j.jhep.2022.10.031

there are safety concerns regarding the use of immune checkpoint inhibition in these patients given the potential for worsening liver injury.[7] The mechanisms leading to monocyte reprogramming and immune checkpoint overexpression are not yet defined and modulating them to prevent sepsis and to safely promote hepatic regeneration is an unmet clinical need in ALF. Importantly, it was recently proposed that metabolic factors may evoke monocyte reprogramming in acute-on-chronic liver failure (ACLF),[8] but whether this finding extends to ALF remains unknown.

The liver, as a major metabolic organ, is responsible for the metabolism of many exogenous compounds and synthesis of endogenous metabolites. These factors make untargeted metabolomics/lipidomics, as well as more targeted methods (*e.g.* for acylcarnitines, and bile acids[9] as markers of mitochondrial dysfunction and hepatotoxicity, respectively) a useful approach for functional investigations. This was recently highlighted in studies of paracetamol-related ALF by providing a means of gaining a metabolic signature of disease and for highlighting pathways for mechanistic and therapeutic exploration.[9]

More recently the prognostic role of lysophosphatidylcholines (LPCs) in ACLF, and their potential in monocyte functional modulation has been shown.[8] Lysophosphatidylcholinic acid (LPA) and LPC are the most studied lysoglycerophospholipid species modulating acute and chronic inflammatory processes. LPAs originate from the hydrolysation of membrane phospholipids, including phosphatidylcholine (PC), phosphatidylethanolamine, and phosphatidylserine, to lysophospholipids. This process is catalysed by phospholipases A1 (PLA1) and 2 (PLA2). Then a lysophospholipase D, named autotaxin (ATX), converts LPC to LPA.

The LPC-ATX-LPA axis has been reported to exert its effect through LPA1-3 receptors and LPA4-6 receptors that belong to the endothelial gene and non-endothelial gene families respectively.[10]

These receptors are of clinical significance, for example specific LPAR4 deletion improved inflammatory cell recruitment in atherosclerotic lesions.[11,12] Similarly, lysoglycerophospholipids have been reported as active mediators in rheumatoid arthritis, with increased LPA and LPAR1 levels observed in affected patients. Moreover, LPAR1 antagonism modulated synovial inflammation and bone and cartilage damage.[13,14] LPARs are implicated in neuropathic pain,[15] renal, liver and pulmonary fibrosis and intimal hyperplasia, which is responsible for atherosclerosis.[16]

Although well studied in other inflammatory diseases, large clinical studies linking immunometabolic factors and the LPC-ATX-LPA axis in human ALF have not been undertaken. There is evidence in mice that LPA could be protective against paracetamol (acetaminophen)-induced liver injury[17] while LPC induced lobular hepatitis in another animal model.[18] In liver biopsies from organs donated after circulatory death, LPCs were increased and this was associated with ischaemic liver injury.[19] Moreover, LPCs were associated with early allograft dysfunction post-liver transplant[20] but little is known about the role of lysophospholipids in the acute setting that often leads to liver transplantation.

This present work addresses a gap in our understanding of immunometabolism in ALF. The aim of this research was to (i) investigate the metabolic signature and the immunometabolic role of the LPC-ATX-LPA pathway in order to find a mechanistic explanation for monocyte behaviour in ALF and (ii) identify possible therapeutic target(s) to modulate the systemic immune response in ALF.

Materials and methods

Study population

The exploratory cohort included individuals with ALF recruited at King's College Hospital in London between December 2012 and July 2015 ("Gut-Liver Axis in Acute and Chronic Liver Failure Syndromes and Transplantation"; London -Westminster Research Ethics Committee No.: 12/LO/1417; IRAS No.: 104301). The validation cohort included patients admitted from May 2013 to December 2021 to King's College Hospital using the same exclusion criteria (pregnancy, disseminated malignancy, pre-existing immunosuppressive states including drugs and HIV infection and chronic granulomatous diseases). Patients were screened and approached for recruitment as part of the "Monocyte and macrophage phenotype and function in sepsis, acute hepatic failure and chronic liver disease" (London-Westminster Research Ethics Committee No.: 12/LO/0167, IRAS No.: 87203) and the "Immunometabolism in Sepsis, Inflammation and Liver Failure Syndromes/IMET" (North West Haydock Research Ethics Committee No.: 19/NW/0750, IRAS No.: 244089) studies within 24 h of admission. Patients or family consultees in case of lack of capacity provided written informed consent. Clinical data and laboratory parameters were collected, and disease severity and prognostic scores were calculated, including model of end-stage liver disease (MELD), Child-Pugh, and Sequential Organ Failure Assessment (SOFA)[21] (see Tables S1 and S2).

Isolation of plasma and human peripheral blood mononuclear cells

Blood was drawn into lithium heparin Vacutainers (BD, Franklin Lakes, NJ) and peripheral blood mononuclear cells (PBMCs) isolated as per supplementary materials and methods.

Proton nuclear magnetic resonance (^{1}H NMR) spectroscopy

^{1}H NMR spectroscopy was initially used to profile plasma and identify the main metabolite groups perturbed in ALF. Please see supplementary materials and methods for details.

Untargeted UPLC-MS lipid analysis

Ultraperformance liquid chromatography-tandem mass spectrometry (UPLC-MS) was employed using an untargeted method to generate lipid profiles from serum in both positive and negative ionisation modes.[22] Please see supplementary materials and methods for details.

UPLC-MS - BIOCRATES p180 assay

We utilised the AbsoluteIDQ® p180 kit (Biocrates Life Sciences, Austria) to quantify 180 known metabolites as previously described.[8] Please see supplementary materials and methods for details.

Cytokine analysis and ELISAs

Plasma cytokines (*IFN-γ, IL-1β, IL-2, IL-4, IL-6, IL-8, IL-10, IL-12p70, IL-13, TNFa*) were measured using V-PLEX Proinflammatory Panel 1 Human Kit (Meso-Scale Discovery,Rockville, MD). ATX, PLA1, PLA2, OPN and M30 were quantified with ELISA as per supplementary materials and methods.

Single-epitope enzymatic immunohistochemistry for detection of ATX-positive cells

Liver tissue from explants was stained with primary antibody ENPP2 (Abcam # ab77104, UK). Please see supplementary materials and methods for details.

Cell culture

Isolated PBMCs from both HCs and individuals with ALF were incubated with different lipids (LPA 16:0, LPA 18:0, LPA 18:1, LPC 16:0, LPC 18 - Avanti Polar Lipids, Alabaster, AL) and LPAR antagonists H2L518630 (Sigma-Aldrich), Ro 6842262(Bio-techne) or Ki 16425 (Sigma-Aldrich). Please see supplementary materials and methods for details.

Immunophenotyping

Monocyte phenotype was determined by flow cytometry on PBMCs using the antibodies in Tables S3 (see supplementary materials and methods).

Monocyte total RNA isolation and mRNA sequencing

Please see supplementary materials and methods for details.

Statistical analysis

Please see supplementary materials and methods for details.

Results

As detailed in the Methods section, the exploratory cohort included 34 individuals with acute liver disease (7 acute liver injury [ALI] and 27 ALF), 40 HCs, 13 with stable cirrhosis, and 50 with acute decompensation of cirrhosis (AD). Transplant-free survival rates at 28 and 90 days and 1 year for ALF were 67%, 56% and 52%, respectively (Tables S1). The validation cohort consisted of 62 individuals with ALF, 31 HCs, 41 individuals with stable decompensated cirrhosis (according to PREDICT definition[23]), and 31 with sepsis (according to SEPSIS-3 criteria).[21] A sub-cohort was used for metabolomics/lipidomics (Tables S2). The transplant-free survival rate of individuals with ALF was 56% at both 28 and 90 days.

AD and ALF are metabolically different from HC according to multivariate analysis of 1H NMR spectroscopic data

In the exploratory cohort, a three-component principal component analysis (PCA) model of acute liver disease and HCs (R^2 = 0.48; Q^2 = 0.38), produced from the data obtained from the ^{1}H NMR spectroscopic analysis of plasma, showed a clear separation between HC and ALI/ALF scores in PC2 which explained 29% of the total variance for the model (Fig. 1A,B). The PCA loading revealed a decrease in lipid resonances (LDL, VLDL and phosphatidylcholine), as well as a decrease in the branched-chain amino acids isoleucine and valine and increased lactate, formate and the amino acids lysine, glycine, glutamine and the aromatic amino acids tyrosine and phenylalanine (Fig. 1B) compared to HCs.

The ALF samples that lay outside the Hoteling's ellipse, and that were separated from all other samples in PC1, also revealed the presence in the plasma ^{1}H NMR spectra of drug-related compounds, such as sedative and anaesthetic agents, being administered to critically ill patients receiving intensive care.

Untargeted UPLC-MS lipidomic analysis showed reduced LPCs in individuals with ALF

A previous ^{1}H NMR spectroscopy and UPLC-MS study from our group identified LPCs as the main lipid class driving change seen in survivors *vs.* non-survivors in those with AD.[24] Based on these findings, an untargeted UPLC-MS lipid profiling method[22] was applied to sera from the exploratory cohort of patients (Fig. 1C). Data were acquired in both positive and negative ESI modes and both sets of data were subjected to multivariate statistical analysis.

PCA modelling of HC and ALF-derived MS results revealed a distinct separation between HC and ALF for both the positive (Fig. 1D, two component model, cumulative R^2 = 0.59; Q^2 = 0.52) and negative ESI data (Fig. 1E, two component model, cumulative R^2 = 0.59; Q^2 = 0.52). Multivariate modelling using OPLS-DA (orthogonal projections to latent structures discriminant analysis) was performed comparing survival at 30 and 90 days and 1-year post admission. All analysis performed on ALF and ALI groups produced invalid models to predict mortality with low or negative Q^2Y values for 30, 90 and 1-year post admission (data not shown).

Following multivariate statistical analysis, 34 discriminating features (Tables S4), selected from S-plots and VIP (variable importance in projection) plots for ALF *vs.* HC, were subjected to tandem mass spectrometry (MS/MS). Furthermore, 70 features with the highest overall intensities were also subjected to MS/MS (Tables S5). Fragmentation data generated by MS/MS were used to confirm the tentative IDs matched to database searches.

In this way, the identities of four of the discriminating features (LysoPC(14:0) $[M+H]^+$, LysoPC(18:1) $[M+H+H_2O]^+$, LysoPC(16:1) $[M+H+H_2O]^+$) were confirmed. Pairwise comparisons of ALF *vs.* HC show a decrease in LysoPC(14:0), LysoPC(18:0), LysoPC(18:1), LysoPC(18:2), PC(18:0/20:3), PC(18:1/20:5), sphingomyelin (SM) (d16:1/18:1), SM(d16:1/24:1), SM(d18:1/16:0), SM(d18:1/22:1), SM(d18:1/24:0) and TG(18:2/18:2/18:3) and an increase in PC(14:1/18:0), PC(16:1/18:2) and LPA(18:0e/0:0) in individuals with ALF compared to HCs. A decrease in LysoPC(16:0) was common to all liver diseases (stable cirrhosis, AD, ALI and ALF) compared to HCs.

Hierarchical cluster analysis of lipids identified from UPLC-MS data

Lipids were further assessed to determine correlation patterns in ALF. Correlation heatmaps were computed from the identified positive ESI lipid $\log_{10}$ transformed data, using Pearson correlation r^2 (colour scale of -0.5-1.0) separately for HCs (Fig. 1F), acute liver disease (Fig. 1G) and cirrhosis (Fig. 1H).

Four main clusters of lipids were determined from metabolite-metabolite correlation analysis of the HC group. In

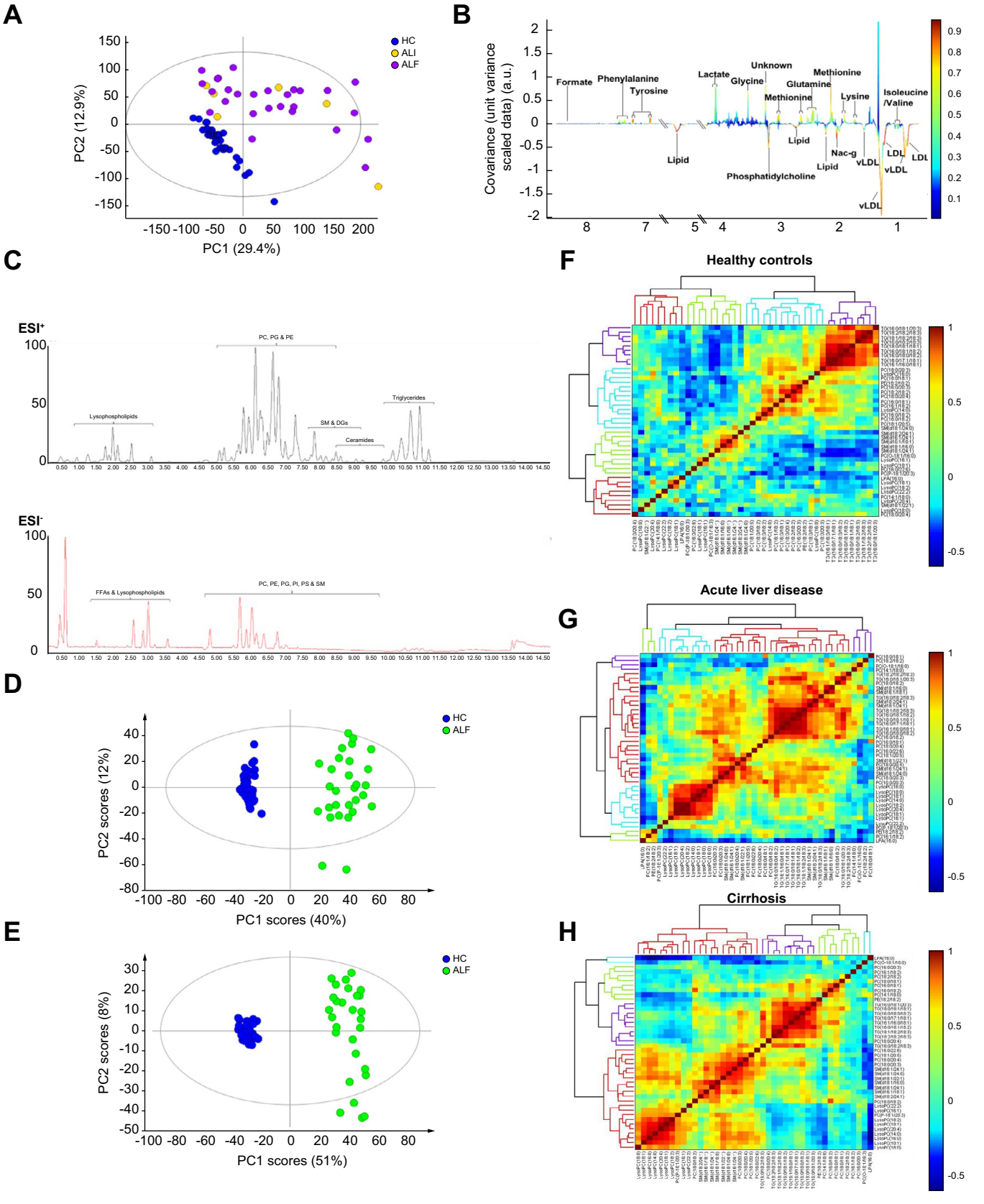

Fig. 1. ^{1}H NMR spectroscopic and chromatographic data. (A,B) Multivariate analysis of ^{1}H NMR spectroscopic data: ALI and ALF are metabolically different from HC. In the exploratory cohort, a three-component PCA model of acute liver disease and HCs (R2 = 0.48; Q2 = 0.38), showed a clear separation between HC and ALF scores in PC2 which explains 29% of total variance for the model. The PCA loading revealed a decrease in lipid resonances (LDL, VLDL and phosphatidylcholine), as well as a decrease in the BCAAs isoleucine and valine and raised amounts of lactate and formate and the amino acids lysine, glycine, glutamine and the AAAs tyrosine

the purple cluster, eight triglycerides (TGs) showed a strong intercorrelation (r^2 >0.7). In the blue cluster there was a strong correlation between phosphocholines (r^2 >0.6). Furthermore, PC(16:0/18:1), LysoPC(14:0), PC(16:0/18:2) were correlated with PC (18:0/20:3), TG (16:1/16:0/18:1) and TG (16:0/17:1/18:1) (r^2>0.7). Within the green cluster there was a strong correlation between SMs including SM(d16:1/24:1), SM(d16:1/18:1), SM(d18:1/24:1) (r^2 >0.6).

Two main clusters were revealed in the correlation heatmap from the acute liver disease (ALI and ALF) groups. In the red cluster, 6 TGs were highly correlated (r^2 >0.8). Also, in the red cluster, SM(d18:1/24:1), SM(d18:2/24:1), SM(d16:1/18:1), SM(d18:1/16:0) were correlated (r^2 >0.7). In addition, SM(d16:1/24:1), SM(d18:1/24:0), PC(18:0/20:3) and PC(16:0/20:3) also from the red cluster were correlated (r^2 >0.8). Seven LPCs in the blue cluster were correlated (r^2 >0.8).

Three main clusters were found in the correlation heatmap from the cirrhosis group. Eight triglycerides were correlated (r^2 >0.8). Furthermore, 7 LPCs were correlated (r^2 >0.8). In addition, PC(18:0/20:3), SM(d16:1/24:1), SM(d18:1/24:0), SM(d18:1/22:1) and SM(d18:1/16:0) were also highly correlated (r^2 >0.8) and SM(d18:1/16:0), SM(d18:1/24:1), SM(d16:1/18:1) and SM(d18:2/24:1) were highly correlated (r^2 >0.8) as well.

Overall, metabolite correlations within the LysoPC and SM groups intensified in both cirrhosis and acute liver disease compared to HCs.

LPC 16:0 was highly discriminant between ALF and HC

In order to confirm our preliminary data, targeted metabotyping (Biocrates Absolute IDQp180) was performed on plasma from the validation cohort, including 43 individuals with ALF, 24 HCs, 21 individuals with stable decompensated cirrhosis, and 31 with sepsis (as proinflammatory control). Unsupervised multivariate analysis using PCA and supervised OPLS-DA identified LPC 16:0 as highly discriminant between ALF and HC together with glutamine, alanine, and the PCs 34:2, 36:2 and 36:3 (R2X 0.592; R2Y 0.666, Q2 0.613, AUROC 0.969961) (Fig. 2A,B,D). From enrichment analysis, phospholipid biosynthesis was the principal pathway differentiating ALF from HC (Fig. 2C) and cirrhosis but not from sepsis (Fig. S2). Moreover, LPC 16:0 remained relevant (within the top 10 metabolites identified with VIP) when samples were analysed using SOFA score as Y in a PLS model (R2X 0.645; R2Y 0.677; Q2 0.599; p = 4.17616e-22), highlighting the correlation with the severity of the disease (Fig. 2E).

LPCs are prognostic markers of poor outcome in ALF

Univariate analysis showed a reduction of LPC 16:0, 18:0 and 18:1 in individuals with ALF compared to HCs and those with cirrhosis (Fig. 3A). Moreover, individuals with poor prognosis (dead or transplanted at 90 days) had the lowest relative amounts of these lipids, *e.g.* for LPC 16:0 and LPC 18:1 p <0.05 (Fig. 3B). Furthermore, the amounts of these LPCs were negatively correlated with MELD score (Fig. S1). Both for ALF and sepsis, no difference was found in the quantities of LPCs observed according to the presence of one particular organ failure (namely renal, circulatory and respiratory) (Fig. S1F).

ATX and PLA2 were increased in the plasma of individuals with ALF

In order to explore the source of reduced LPC concentrations in plasma, we studied the main enzymes involved in their metabolism. There was an increase in ATX (ALF *vs.* HC p <0.001) and its product LPA in ALF compared to both HCs and those with sepsis (ALF *vs.* HC p <0.01). PLA1 was also increased in all diseases (cirrhosis, ALF and sepsis), however PLA2 was only increased in ALF *vs.* cirrhosis, and *vs.* HCs (p <0.0001) (Fig. 3C). Taken together these findings suggest a potential role for ATX-mediated conversion of LPC into LPA in the liver.

Hepatic ATX expression was increased in ALF

In explants from individuals with ALF of different aetiologies, ATX expression was observed in areas of viable hepatocytes sparing necrotic areas (Fig. S2). This suggests a role for hepatocytes in the conversion of LPC to LPA.

Individuals with ALF showed a markedly enhanced cytokine response and increased circulatory makers of cell death

Similarly to sepsis, plasma from individuals with ALF contained increased amounts of both proinflammatory (IL-6, IL-8, TNFa) and anti-inflammatory cytokines (IL-10) compared to that from HCs and those with cirrhosis (Fig. 4 and Table S1). Interestingly OPN, a highly modified integrin-binding extracellular matrix glycophosphoprotein produced by the cells of the immune system and a mediator of hepatic macrophage infiltration,[25] was increased in ALF compared to sepsis (p <0.01), confirming a role in hepatic inflammation. M30, a caspase-cleaved cytokeratin 18 fragment produced during apoptosis, was increased in individuals with ALF compared to HCs (Fig. 4C) and directly correlated with proinflammatory cytokines (Fig. 4B). The LPCs 16:0 and 18:0 were directly correlated with lymphocyte count, IL-10, IL-6, IL-8 and IL-1β and inversely with monocyte and neutrophil counts (Fig. S1D).

CD14$^+$ monocytes in ALF have a pro-restorative profile with increased MerTK and PD-L1 expression

Phenotypic characterisation of PBMCs by flow cytometry showed increased expression of MerTK and PD-L1 in CD14+ monocytes from individuals with ALF compared to HCs (Fig. 5A-B, complete phenotyping gating strategy is shown in Fig. S3A). Both markers were highly expressed in the

and phenylalanine (B) compared to HCs. (C) BPI chromatograms of QC serum in ESI+ and ESI- ionisation modes. (E,D) PCA modelling of HC and ALF for both positive and negative ESI data, revealed a distinct separation between HC and ALF for both positive (D, two component model, cumulative R2 = 0.59; Q2 = 0.52) and negative mode data (E, two component model, cumulative R2 = 0.59; Q2 = 0.52). (F–H) Correlation heatmaps from the identified positive ESI lipid. The lipids detected in positive ESI were further assessed to determine correlation patterns in acute (ALI and ALF) liver disease, as performed previously for the ^{1}H NMR spectral data and the UPLC-MS-detected amines. Correlation heatmaps were computed from the identified positive ESI lipid log10 transformed data, using Pearson correlation r2 colour scale of -0.5-1.0, separately for HC (F), acute liver disease (G) and cirrhosis (H). ^{1}H NMR, proton nuclear magnetic resonance; AAA: aromatic amino acid; BCAA: branched-chain amino acids; BPI, base peak intensity; DG, diacylglycerol; ESI, electrospray ionization; FFAs, free fatty acids; PC, phosphatidylcholine; PCA, principal component analysis; PE, phosphatidylethanolamine; PG, phosphatidylglycerol; PI, phosphatidylinositol; PS, phosphatidylserine; QC, quality control; SM, sphingomyelin.

Active lipids modulate monocytes in ALF

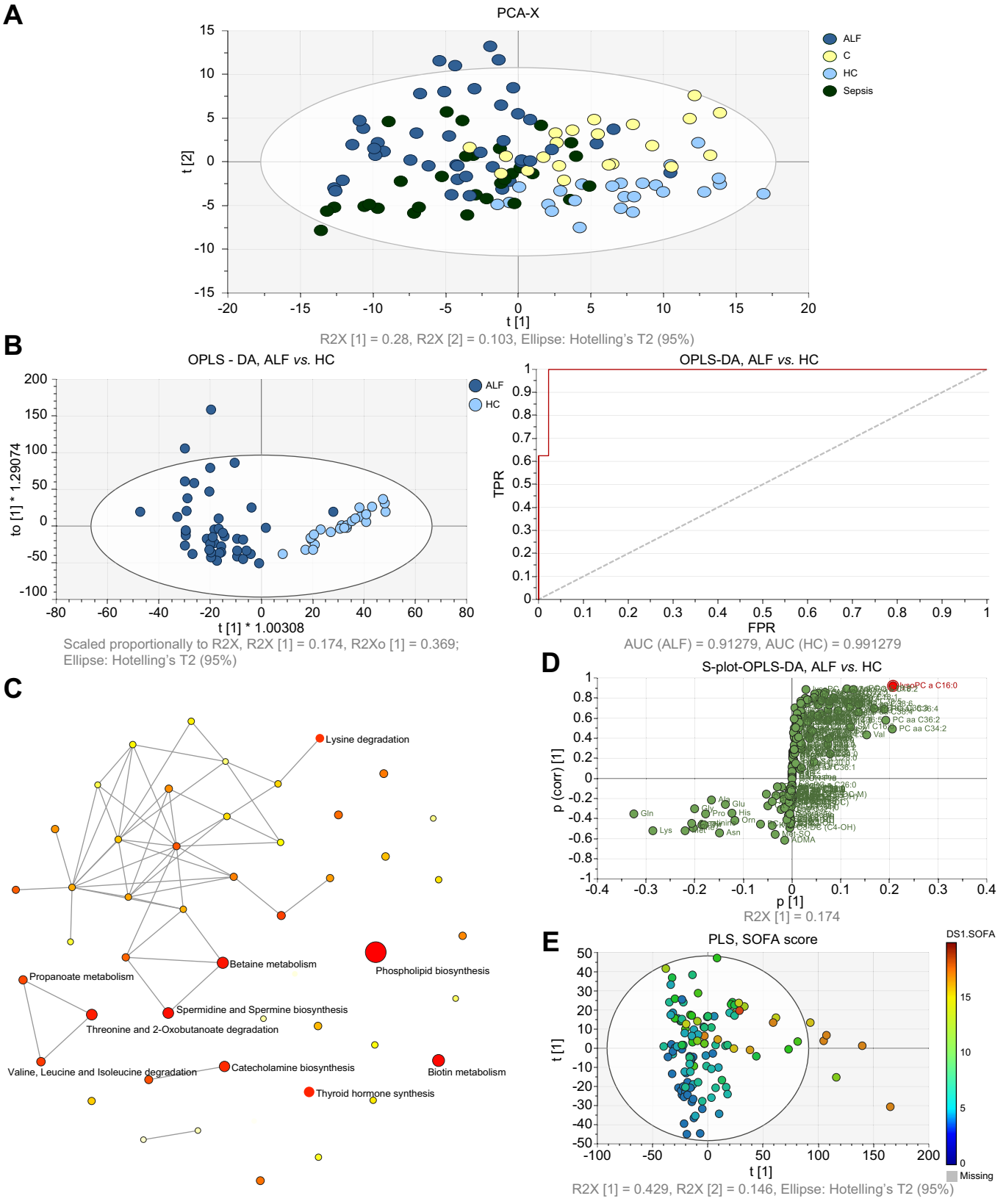

Fig. 2. Discriminative power of LPCs. (A,B) Validation cohort 180-metabolite panel (Biocrates) confirmed the discriminating power of LPCs. In order to confirm our preliminary data, targeted metabotyping was performed on plasma from the validation cohort including 43 individuals with ALF, 24 HCs, 21 individuals with cirrhosis, and 31 with sepsis (as proinflammatory control). PCA and OPLS-DA identified LPC 16:0 as highly discriminant between ALF and HCs together with glutamine, alanine, phosphatidylcholine 34:2, 36:2, 36:3 (R2X 0.592; R2Y 0.666, Q2 0.613, AUROC 0.969961). (C) Enrichment analysis showed phospholipid biosynthesis as the principal pathway differentiating ALF from HC. (D) S-Plot confirmed LPC 16:0 as highly discriminant between HCs and ALF. (E) LPC 16:0 is related to the severity of ALF. When samples were analysed using SOFA score as Y in a PLS model, LPC 16:0 remained in the top 10 metabolites identified with VIP, highlighting the correlation with disease severity. ALF, acute liver failure; HC, healthy control, LPC, lysophosphatidylcholine; OPLS-DA, orthogonal projections to latent structures discriminant analysis; PCA, principal component analysis; PLS, partial least squares; VIP, variable importance in projection.

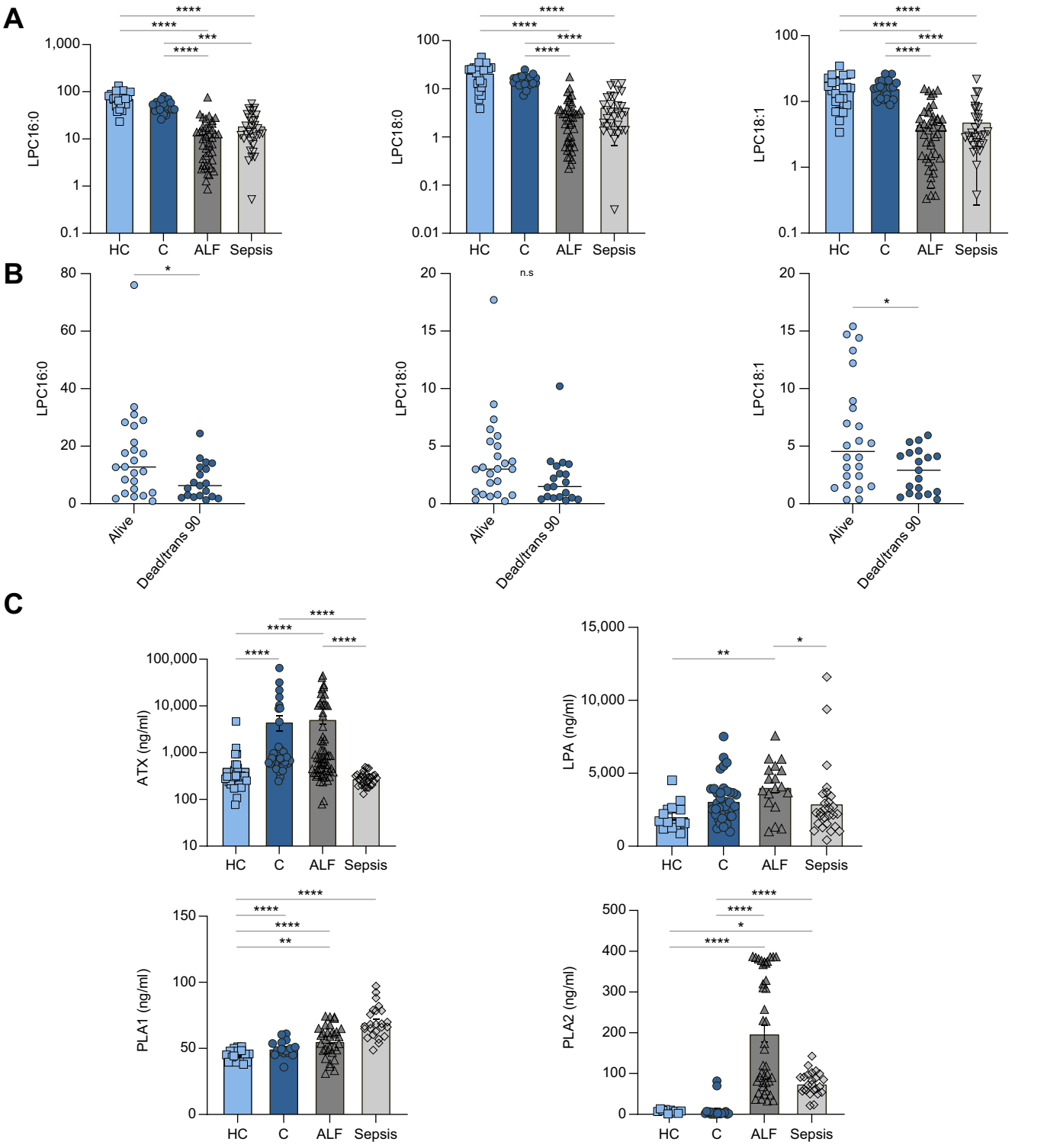

Fig. 3. Prognostic significance of LPC. (A) LPC is significantly reduced in ALF compared to HC and C but not sepsis. Kruskall-Wallis test: HC n = 24, C n = 21, ALF n = 43, Sepsis n = 31. HC *vs.* ALF ****p <0.0001. Graphs show mean +SEM. (B) LPC 16:0, LPC 18:0 and LPC 18:1 were reduced in those with poor prognosis (dead or transplanted at 90 days post admission). Alive n = 24, dead/transplanted n = 19. Mann-Whitney test: LPC 16:0, *p = 0.0339; LPC 18:0 p = 0.06; LPC 18:1 *p = 0.0434. Graphs show mean +SEM. (C) Autotaxin and PLA2 are significantly increased in ALF. ATX: HC n = 31, C = 41, ALF = 62, Sepsis = 31, Kruskal Wallis, HC *vs.* ALF ****p <0.0001. LPA: HC n = 14, C n = 38, ALF n = 18, Sepsis n = 27, Kruskal Wallis, HC *vs.* ALF ** p = 0.0022. PLA1: HC n = 16, C n = 16, ALF n = 32, Sepsis n = 24, one way ANOVA, HC *vs.* ALF ***p = 0.0006. PLA 2: HC n = 10, ALF n = 40, n = 20, sepsis n = 24, Kruskal Wallis, HC *vs.* ALF ****p <0.0001. Graphs show mean + SEM. *p <0.05, **p <0.01, ***p <0.001, ****p <0.0001. ALF, acute liver failure; ATX, autotaxin; C, cirrhotic patients, HC, healthy control; LPA, lysophosphatidylcholinic acid; LPC, lysophosphatidylcholine, PLA, phospholipase A.

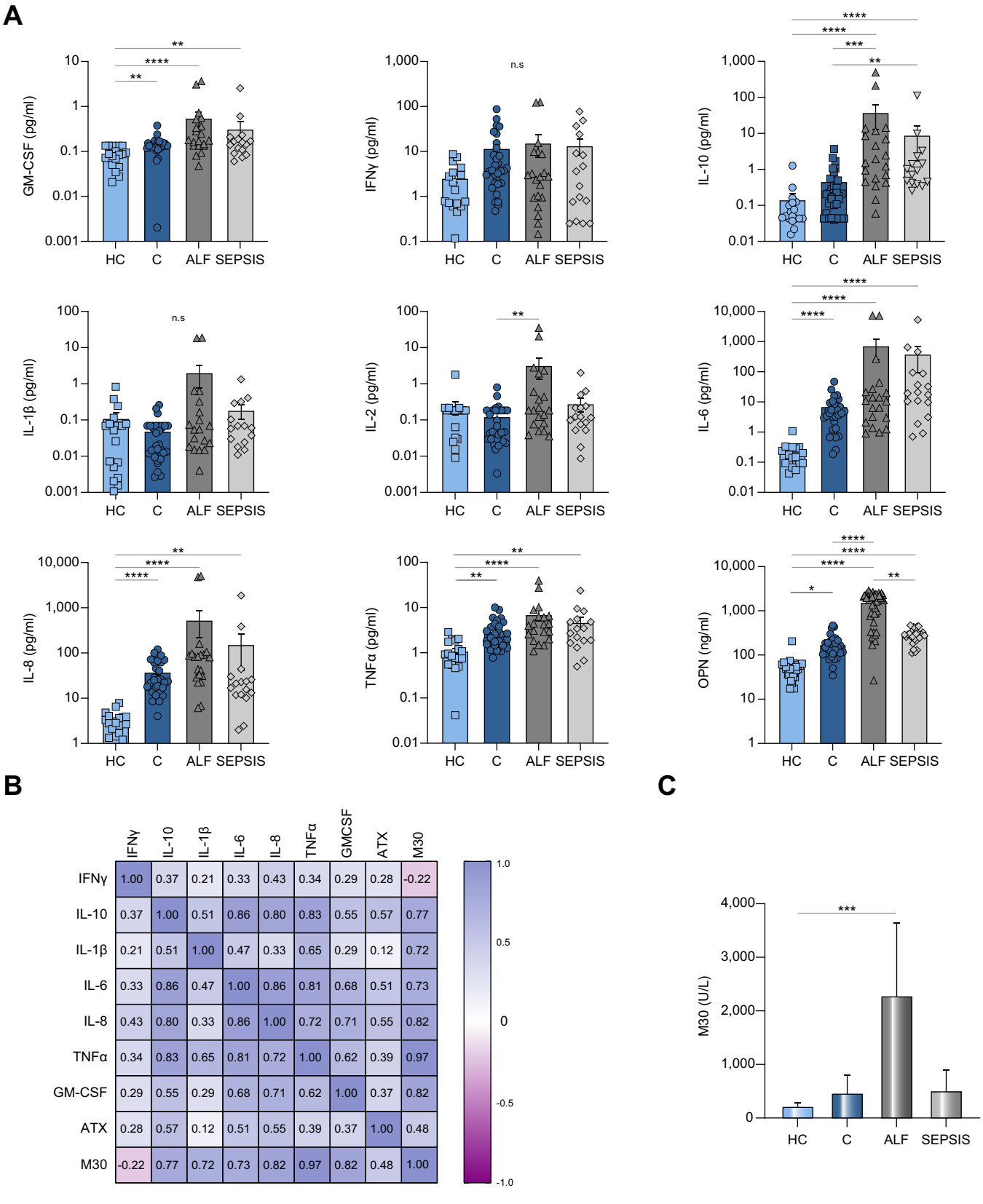

Fig. 4. Increased inflammatory cytokine plasma levels correlate with LPC-ATX-LPA dysregulation in acute liver failure. (A) Individuals with ALF had increased plasma proinflammatory cytokines (validation cohort). HC n = 18, C n = 30, ALF n = 20, sepsis n = 16. Graphs show mean + SEM. Kruskall-Wallis. Most relevant comparisons are shown in detail: HC *vs.* ALF: GM-CSF ****p <0.0001, IFN-γ p >0.9999, IL-10 ****p <0.0001, IL-1β p >0.9999, IL-2 p = 0.7178, IL-6 ****p <0.0001, IL-8 ****p <0.0001, TNFα ****p <0.0001, OPN ****p <0.0001. (B) Correlations Matrix: M30 is directly correlated with proinflammatory cytokines in particular with TNFa. Soluble Mer does not correlate with other immunological markers. Correlation matrix, Spearman's Correlation, correlation coefficients (rho) are shown per pair in the

intermediate $CD14^{+}CD16^{+}$ and classical $CD14^{+}CD16^{-}$ monocyte subsets (Fig. S3B). Immune checkpoint expression on natural killer (NK) and CD56+ T cells did not show a statistically significant difference between study groups (Fig. S4). Notably, we observed an increasing trend of CTLA4-, PD-1- and PD-L1-positive CD56+CD4+T cells (%) in individuals with ALF compared to those with cirrhosis and HCs (Fig. S4B). The percentage of TIGIT expression was increased in ALF CD56+CD8+T and NK cells compared to other groups but again this was not statistically significant.

PBMCs from individuals with ALF were hypo-responsive to LPS/LPC/LPA co-culture

We next decided to test *in vitro* cytokine production and its modulation following lipid treatment (Fig. 5C); therefore, PBMCs were cultured for 24 h and then stimulated with lipopolysaccharide (LPS: 100 ng/ml). Cells from individuals with ALF produced less IL-6 compared to those from HCs (p <0.05). Moreover, LPA 16:0, LPA 18:0, LPA 18:1, LPC 16:0 and LPC 18:0 were also tested as potential modulators of the immune response. The addition of LPAs/LPCs failed to reverse cytokine levels in ALF-derived PBMCs and did not affect HC cytokine production.

LPA 16:0 increases and restores PD-L1 expression and reduces MerTK, CD163 and CD155 expression in monocytes

We next questioned whether *in vitro* LPA treatment of PBMCs from HCs and individuals with ALF would alter their phenotypic characteristics. Following incubation with LPA 16:0, the percentage of $CD14^{+}CD16^{+}$ and $CD14^{+}CD16^{-}$ cells within the monocyte pool was reduced (Fig. 5D). Moreover, after culture with LPA 16:0, LPA 18:0 and LPA 18:1, $CD14^{+}$ monocytes showed immunophenotypic changes (Fig. S5). LPA 16:0 treatment increased monocyte PD-L1 expression (% of positive cells, p <0.05) in ALF samples, that was reduced in untreated conditions compared to HCs (p <0.05), and reduced monocyte MerTK, CD163 and CD155 expression in ALF (% of positive cells and mean fluorescence intensity, p <0.05). Interestingly, no similar effects were observed in T-cell subsets (CD8, CD4, and regulatory) which showed unaltered expression of immune checkpoints following LPA treatment (Fig. S5).

Expression of LPARs in monocytes was upregulated during ALF and their reduction was linked to poor prognosis

Given the potential lipid-mediated modulation of monocyte function, we next sought to examine whether hepatic and monocyte expression of LPA receptors (LPARs1-6) was potentially upregulated. Monocyte expression of LPARs in publicly available microarray data sets was therefore explored. Having already demonstrated increased hepatic expression of ATX and LPAR6 (Gene Expression Omnibus dataset GDS4389, series GSE28619/30) in alcoholic hepatitis and HBV-related ALF,[8,26] we observed a trend toward increased expression of LPAR2, 3 and 6 (GSE120652) in those with ALF resulting from paracetamol overdose.

In vitro stimulation of monocytes with LPS increased LPAR1, LPAR3 and reduced LPAR6 (GSE61298)[27] expression (Fig. S6A). Moreover CD16 -ve monocytes expressed more LPAR1, and LPAR6, and reduced LPAR3 compared to CD16+ve monocytes, confirming a different activation according to monocyte subsets (GSE16836)[28] (Fig. S6B). Also, LPARs were no differently expressed in PBMCs according to the outcome of patients with an acute flare of hepatitis B on chronic infection (GSE168049)[29](data not shown) and in monocyte from patients with paracetamol-induced acute liver failure (GSE80751)[30](Fig. S6C).

LPAR identification with monocyte stimulation by receptor antagonists

From our genetic research, it emerged that LPAR1, 3 and 6 could be involved in the monocyte phenotype changes observed in ALF. To explore which LPAR played a role in the observed effects, fresh PBMCs were stimulated with the antagonists for the three most common receptors (LPARs 1-3); currently there are no commercially available LPAR 4-6 antagonists.

A preliminary study was conducted to decide targets and optimal concentrations of the available antangonists. PBMCs from HCs were cultured with antagonists for LPAR1 (Ro 6842262), LPAR2 (H2L5186303), and LPAR1/3 (Ki 16425). We observed that CD155, CD163, MerTK, PD-1 and PD-L1 were reduced by the LPAR1/3 antagonist (at 1uM) compared to LPA 16:0 (30 uM). This suggests a key role of LPAR1/3 in monocyte phenotype modulation (Fig. S7).

We then focused on LPAR1 and LPAR1/3 antagonism to stimulate ALF cells. LPA 16:0 reduced MerTK and CD163 expression, the effect was statistically significant in HCs and a clear trend was also evident in ALF (Fig. 6). Treatment of PBMCs with LPAR1 and LPAR1/3 antagonists restored the MerTK and CD163 expression reduced by LPA 16:0 treatment.

Taken together these data suggest that an LPAR1/3 mechanism underpins the effect of LPA on the regulatory phenotype of monocytes and these receptors are a target for immunotherapy in ALF.

RNA sequencing showed potential pathways of interest unique to ALF

Finally, to explore pathways linking monocyte function and lipid metabolism, we performed mRNA sequencing on isolated monocytes from individuals with ALF, with decompensated cirrhosis (DC) and HCs (Fig. 7A). As shown in the Venn diagram, 206 genes were unique to ALF (Fig. 7B). *LPAR1,2,5* and *6* expression levels were not different between study groups

corresponding cell. (C) M30, a caspase-cleaved cytokeratin 18 fragment produced during apoptosis, was increased in ALF compared to HC. Graphs show mean + SD, Kruskall-Wallis test, HC *vs.* ALF ***p = 0.0006. *p <0.05, **p <0.01, ***p <0.001, ****p <0.0001. ALF, acute liver failure; ATX, autotaxin; C, cirrhotic patients; HC, healthy control; GM-CSF, granulocyte macrophage colony-stimulating factor; IFN, interferon; IL, interleukin; LPA, lysophosphatidylcholinic acid; LPC, lysophosphatidylcholine; OPN, osteopontin; TNF, tumor necrosis factor.

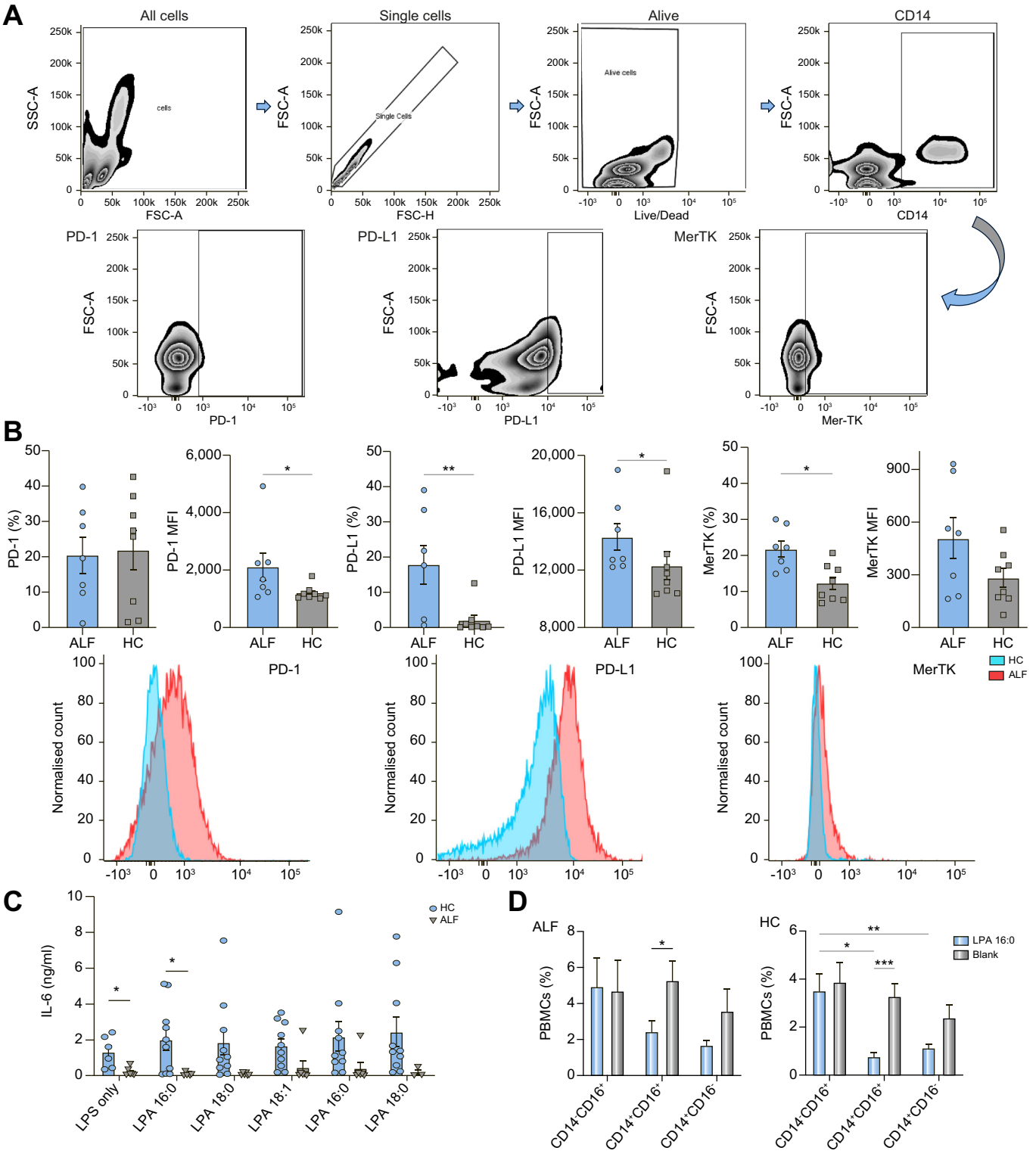

Fig. 5. Monocytes in ALF show a pro-restorative phenotype. (A) Gating strategy, markers including MerTK were assessed on live CD14+ cells. (B) MerTK and PD-L1 expression is increased in fresh CD14+ cells in ALF (n = 7) compared to HC (n = 8). Most relevant comparisons are shown in detail: Mann-Whitney test, PD1% $p = 0.955$, PD1 MFI $^{*}p = 0.0306$, PD-L1% $^{**}p = 0.0059$, PD-L1 MFI $^{*}p = 0.0434$, MerTk % $^{*}p = 0.0140$, MerTk MFI $p = 0.2319$. Graphs show mean +SEM, $^{*}p < 0.05$, $^{**}p < 0.01$, $^{***}p < 0.001$, $^{****}p < 0.0001$. (C) PBMCs from individuals with ALF produced less IL-6 when stimulated with LPS ($p < 0.05$). Moreover, LPA 16:0, LPA 18:0, LPA 18:1, LPC 16:0 and LPC 18:0 were tested as potential modulators of immune response. The addition of LPAs/LPCs failed to reverse the immune dysfunction in ALF PBMCs and did not affect HC function. Mixed effects analysis. Most relevant comparisons are shown in detail: HC *vs.* ALF: LPS only $^{*}p = 0.0135$, LPA 16:0 $^{*}p = 0.0309$. The other comparisons were not statistically significant with $p > 0.05$. Graphs show mean +SEM, $^{*}p < 0.05$, $^{**}p < 0.01$, $^{***}p < 0.001$, $^{****}p < 0.0001$. (D) LPA modifies monocyte phenotype. Percentage of CD14+ cells decreased after 24 h PBMC co-culture with LPA 16:0. Most relevant comparisons are shown in detail: two-way ANOVA, ALF LPA *vs.* blank, CD14-CD16+ $p = 0.9907$, CD14+CD16+ $^{*}p = 0.0125$, CD14+CD16-$p = 0.1336$. Two-way ANOVA, HC LPA *vs.* blank, CD14-CD16+ $p = 0.8709$, CD14+CD16+ $^{***}p = 0.0001$, CD14+CD16-$p = 0.0693$. Graphs show mean + SEM, $^{*}p < 0.05$, $^{**}p < 0.01$, $^{***}p < 0.001$, $^{****}p < 0.0001$. ALF, acute liver failure; HC, healthy control; LPA, lysophosphatidylcholinic acid; LPS, lipopolysaccharides, Mer-Tk, Mer tyrosin kinase; PD-1, programmed cell death protein 1; PD-L1, programmed death-ligand 1.

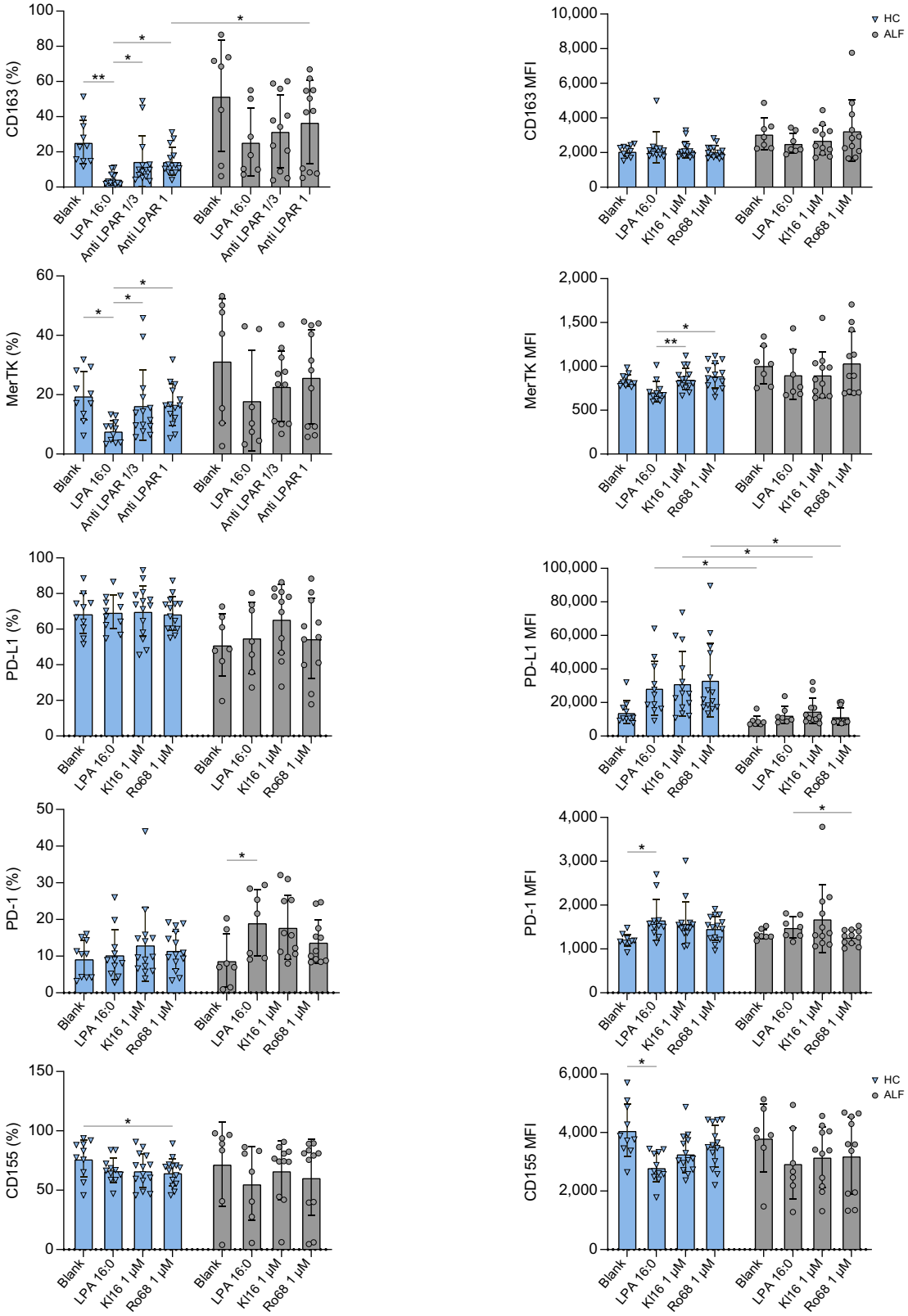

Fig. 6. LPAR1 and 3 were the key receptors leading to LPA-induced monocyte phenotypical changes. In PBMC culture, LPA 16:0 reduced MerTK and CD163 expression in CD14+ cells. Treatment with LPAR1 and LPAR1/3 antagonists restored MerTK and CD163 expression, which had been reduced by LPA 16:0 treatment. Mixed effects analysis. Most relevant comparisons are shown in detail: HC LPA 16:0 *vs.* Ki 16425, CD163% *p = 0.0215, MerTK% *p = 0.0276, MerTk MFI *p = 0.0197. HC LPA 16:0 *vs.* Ro 6842262, CD163% *p = 0.0225, MerTK% *p = 0.0266, MerTK MFI *p = 0.0442. Graphs show mean +SEM, *p <0.05, **p <0.01, ***p <0.001, ****p <0.0001. MerTK, Mer tyrosine kinase, PD1, programmed cell death 1, PD-L1, programmed cell death ligand-1.

Active lipids modulate monocytes in ALF

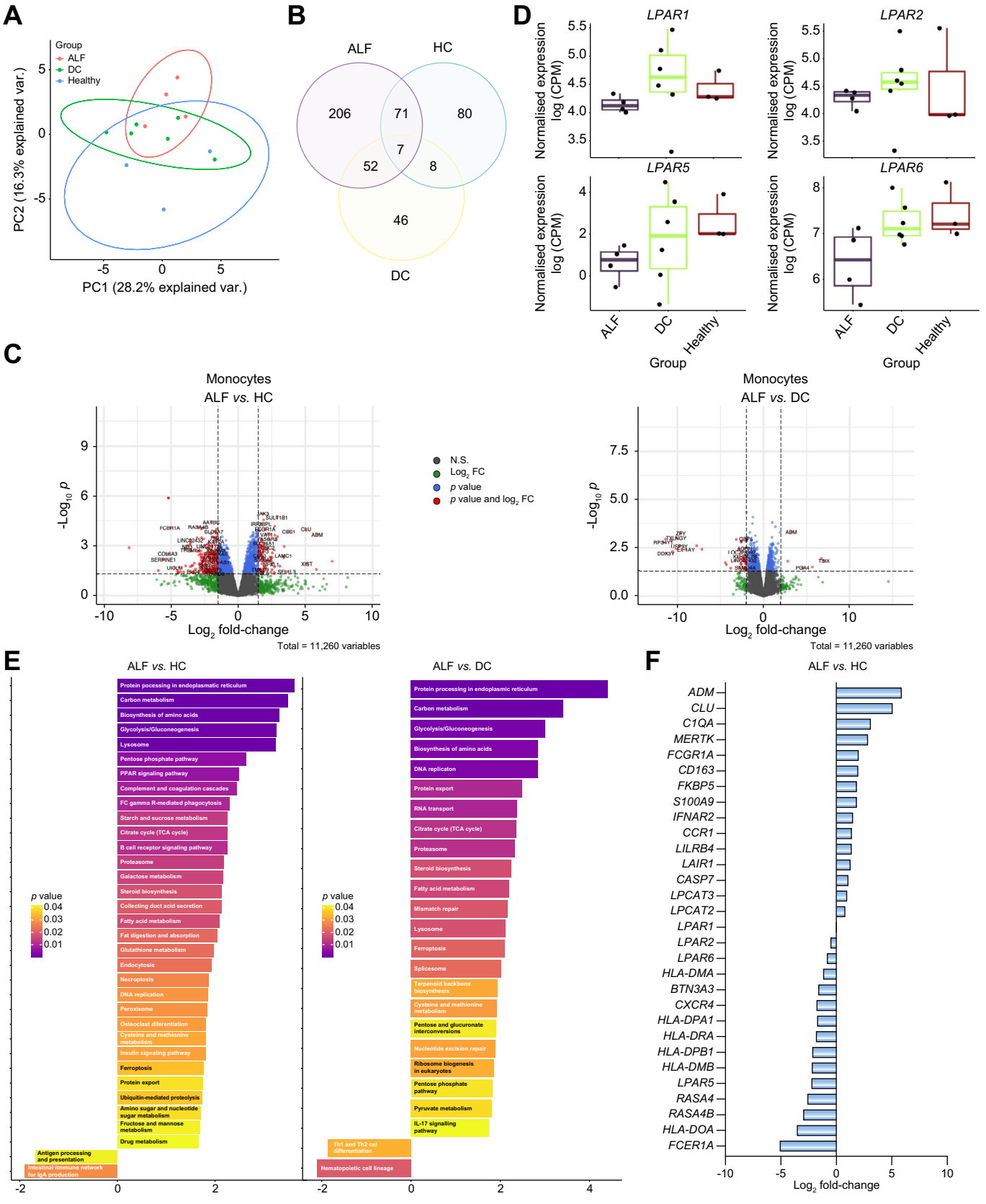

Fig. 7. RNA sequencing of monocytes unveiled pathways of interest in ALF. (A) Principal component analysis for RNA sequencing data showing the three study groups: ALF (n = 4), DC (n = 6) and HC (n = 3). (B) A Venn diagram showing the overlap of differentially expressed genes between the three different pairwise comparisons using p <0.05 and |logFC|>1.5. (C) Volcano plots showing the differential expression in Log2 fold change of genes between ALF *vs.* HC and ALF *vs.* DC. (D) Box plots of LPAR genes of interest in ALF, DC, HC, LPAR3 and four were detected but filtered out due to low expression levels. Kruskall-Wallis, not significant.

(Fig. 7C-D), while *LPAR3* and *LPAR4* genes were filtered out due to low expression levels (data not shown).

Of note, *MerTK* and *CD163* monocyte transcript levels were increased in ALF compared to control while HLA appeared hypo-expressed in ALF, and the antigen processing and presentation pathways were downregulated (Fig. 7E). *HLA-DPA1, HLA-DPB1, HLA-DRA* and *HLA-DMB* were uniquely downregulated in ALF compared to both groups, while *CD163, IFNAR 2, FKBP5, ADM* were upregulated in ALF only (Fig. 7D and F). Moreover, *LAIR1* and *LILRB4*, coding for leucocyte inhibitory receptors, were upregulated in individuals with ALF compared to both HCs and those with DC. Among the main pathways discriminating between ALF *vs.* HCs and *vs.* DC we found genes related to lipid metabolism including fatty acid metabolism and steroid metabolism, in particular *LPCAT2* and *LPCAT3* which were upregulated in ALF.

Ingenuity pathway analysis by Qiagen IPA (Fig. S8) showed the possible relationship between LPARs and monocyte markers. Several pathways were putatively identified, and further research is needed to better explain how to safely modulate monocyte function.

Discussion

Our study is the first to demonstrate the upregulation of the LPC-ATX-LPA axis in both peripheral blood and liver tissue in ALF and its link, via an LPAR1/3-related mechanism, with the immune phenotype modulation of circulating monocytes.

We report a crucial role of lipid metabolism in ALF. LPCs 16:0 and 18:1, which form the most abundant LPC species in plasma, were identified as discriminant in a population of individuals with ALF when compared to HCs following unbiased ^{1}H NMR spectroscopic and LCMS-based analysis of peripheral blood. These lipids were predictive of poor prognosis in the same population (including mortality or liver transplant at 90 days) and the levels were inversely correlated with MELD score. However, no relationship was found with other organ failures, *e.g.* renal, circulatory and respiratory systems.

Inflammation is accepted as the driving mechanism leading to multiorgan failure and death in ALF populations,[31] and monocyte and macrophage dysfunction are central to disease pathogenesis and progression.[2] Initial activation of liver-resident macrophages (Kupffer cells) by damage-associated molecular patterns leads to monocyte recruitment and infiltration. Such effects on monocytes may then contribute to local tissue destruction during the propagation phase and result in the secretion of proinflammatory cytokines.[32,33] In parallel anti-inflammatory cytokines (*i.e.* IL-10) were increased, suggesting the activation of a compensatory anti-inflammatory response syndrome in ALF.[2]

In our cohort, proinflammatory cytokines increased more than sixfold compared to controls (Fig. 4) and were correlated with markers of cell death (M30). Subsequently, the recruited monocytes matured into macrophages following local reprogramming towards resolution responses (to promote tissue integrity).

Intrahepatic events may also affect circulating monocytes, which show numerous acquired defects in ALF syndromes, with dysfunctional antimicrobial activity and increased susceptibility to sepsis.[2] What contributes to such reprogramming has been a matter of debate and many soluble mediators have been proposed.[2,34]

Herein, we have shown that such soluble mediators could include lipids in the LPC and LPA families. The LPCs are lipid metabolites of PC, synthesized by various enzymes including secretory PLA2, HDL-associated lecithin-cholesterol acyltransferase in the reverse cholesterol pathway, as well as hepatic and endothelial lipase.[35].

LPAs are thought to be bioactive molecules and their function is exerted by extracellular signalling through at least six (LPAR1-6) 7-transmembrane G protein-coupled receptors.[36]

There are two major synthetic pathways for LPAs.[36] Lysophospholipids can be converted to LPA via ATX activity or, alternatively, phosphatidic acid is first produced from phospholipids via phospholipase D, or from diacylglycerol through diacylglycerol kinase, and then converted directly to LPA by the actions of either PLA1 or PLA2.

Both pathways appear to be activated in ALF since ATX and PLA2 were increased compared to controls. However, ATX has been found in liver explants obtained from individuals with ALF, confirming the central role of the liver in the dysregulation of the LPC/ATX/LPA axis in ALF. That this is not purely due to systemic inflammation is evidenced by the lack of ATX increases in individuals with severe sepsis.

ALF shares similarities with ACLF, in which cholesteryl esters and lysophospholipids have been considered part of a lipid fingerprint.[37] In addition, PBMC transcriptome analysis has revealed metabolic alterations, including the upregulation of the PPAR signalling pathway, cholesterol metabolism, sphingolipid metabolism and glycosaminoglycan biosynthesis[38] and this was confirmed by our data on monocytes isolated from individuals with ALF.

In this ALF cohort, circulating monocytes showed increased PD-L1 and MerTK expression, confirming a pro-restorative phenotype, previously associated with immunoparesis and increased susceptibility to infections.[2,3,5] Moreover, no significant phenotypic differences were found in blood NK and CD56+T cells in ALF, but this could also be attributed to the early time of sampling. In our recent data from a murine model of paracetamol overdose, PD-1 expression in T-cell subsets remained unaltered during the first 3 days after the acute insult. However, PD-L1 expression in regulatory T and NKT cells was upregulated at 72 h post paracetamol overdose, during the pro-restorative phase.[3]

We demonstrate a switch in monocyte populations, with a reduction in CD14+ cells with LPA *in vitro*. Moreover, among LPA 16:0, 18:0 and 18:1, the former induced profound phenotypic changes *in vitro*, reducing CCR2, CD163, CD155 and MerTK and increasing PD-L1 expression in both HCs and individuals with ALF, without affecting the T-cell population.

LPAR1 $p = 0.2250$, LPAR2 $p = 0.5571$, LPAR5 $p = 0.4340$, LPAR6 $p = 0.4058$. (E) Pathway analysis plots based upon the GAGE analysis for the pairwise comparisons ALF *vs.* HC and ALF *vs.* DC. (F) Differential expression in Log_2 fold change of genes involved in lipid metabolism and immune response. ALF, acute liver failure; DC, decompensated cirrhosis, HC, healthy control; LPAR, lysophosphatidylcholinic acid receptor; PC, principal component.

In order to identify the LPAR responsible for such an effect, we examined LPAR expression in monocytes through publicly available microarray data sets. *In vitro*, M1 monocytes have increased LPAR1, LPAR3 and reduced LPAR6, suggesting a proinflammatory role for the first two receptors. This is complementary to the previous finding of increased ATX and LPAR1 and 6 in liver tissue from individuals with alcohol-related liver disease and HBV-related ALF.[8] We then demonstrated that LPAR1/3 antagonism had a similar effect on both cells from HCs and individuals with ALF, reversing the effect of LPA and increasing CD163 and MerTK.

To evaluate if the phenotypic change was consistent with gene expression, we performed RNA sequencing on isolated monocytes from those with ALF, DC and HCs. *LPAR1, LPAR2, LPAR5* and *LPAR6* expression were not statistically different between groups. Thus, we hypothesised that the circulating lipids stimulate the receptors without inducing differential gene expression.

Our numbers were small to analyse outcome prediction; however, from public datasets, we found that in PBMCs from individuals with ACLF secondary to hepatitis B infection and monocytes from those with paracetamol-induced ALF, LPARs were not differently expressed in patients with poor prognosis.

In our cohort, transcript-level expression of *MerTK*, *CD163, LAIR1, LILRB4, S100A9* in isolated monocytes was increased in those with ALF compared to HCs, while MHC-related genes *(HLA-DPA1*[39]*, HLA-DPB1, HLA-DRA, HLA-DOA* and *HLA-DMB*) appeared hypo-expressed in ALF, confirming an immunosuppressive/pro-restorative profile.

S100A9 is a marker of myeloid-derived suppressor cells, a population of cells that can negatively regulate T-cell function.[40] Their role has been studied in cancer[41] and by our group in ACLF,[42] in which myeloid-derived suppressor cells displayed immunosuppressive properties, decreasing T-cell proliferation and reducing bacterial uptake.

Other genes were upregulated only in ALF including ADM (adrenomedullin, a potent vasodilator peptide[44]), IFNAR2 and FKBP5. The latter encodes FKBP51, which acts as a negative transcriptional regulator of the glucocorticoid receptor and a positive regulator of PPAR signalling. This gene is also related to stress and suicidal behaviour,[43] so it will be interesting to explore its role in the setting of ALF and immune dysfunction from paracetamol overdose.

LPS and IFN-γ increase adrenomedullin production by macrophages *in vitro*.[45] Adrenomedullin strongly inhibits LPC-induced migration of human coronary artery smooth muscle cells in a concentration-dependent manner.[46] Its plasmatic concentration has been correlated with vasopressor requirements, organ dysfunction, and mortality in sepsis.[47] Moreover, pro-adrenomedullin is associated with short-term survival and ACLF development in individuals with DC,[48] but its role in ALF is unknown.

Among the main pathways discriminating between ALF *vs.* HCs and *vs.* DC we also found genes related to lipid metabolism, including fatty acid metabolism and steroid metabolism. Lysophosphatidylcholine acyltransferase (LPCAT) 2 and 3 genes would be of future interest since they are upregulated in ALF and related to the metabolomic signature we discovered. LPCAT2 has been shown to induce macrophage cytokine gene expression and release in response to TLR4 and TLR2[49] and LPCAT3 seems crucial in the arachidonic acid reacylation pathway[50] and ferroptosis,[51] a novel pathway of iron-dependent necrotic cell death characterised by the accumulation of lipid peroxides. Among the various reactive oxygen species, lipid peroxides are direct inducers of ferroptotic cell death.[52] One of the crucial steps in this pathway is indeed performed by LPCAT3,[53] selectively activated by IFN-γ, which incorporates polyunsaturated fatty acid-CoA into phospholipids, using PCs and phosphatidylethanolamine as substrates. Indeed, the links between lipid metabolism and the immune system are multiple and many lipid mediators have been studied in ferroptosis, including specialised pro-resolving mediators that would be an interesting research focus in ALF.[54]

The aim of the present study was to find potential targets for immunomodulation in ALF. Although ATX has been explored as a target for the treatment of individuals with idiopathic pulmonary fibrosis,[55] the heterogenic distribution and expression profiles of LPARs are such that blocking LPA production globally by inhibiting ATX could lead to severe adverse side effects. Thus, drug development needs to focus on the discovery of novel, potent LPAR ligands targeting a specific receptor subtype without negating the physiological roles of other subtypes.[10] Currently, no drugs targeting LPARs have been approved by the FDA, while several clinical trials are testing LPAR1 antagonists for idiopathic pulmonary fibrosis and systemic sclerosis, and a radioligand that targets the LPAR1 receptor has entered a phase I clinical trial for PET imaging of idiopathic pulmonary fibrosis.[10]

Our research has several limitations. Total LPA only was measured by ELISA rather than individually. The reason is that LPA measurement via LCMS techniques is challenging. LPAs can be generated *ex vivo* after sample collection and are affected by several chemical and biological processes, making their accurate measurement in biological fluids difficult.[56] We are currently optimising a technique to efficiently measure LPAs to overcome this limitation. Moreover, we did not measure free and total LPA/LPC, thus the role of albumin binding was not explored in this study.

We used LPS as an immunogenic stimulant and thus only TLR4-mediated inflammation was explored. Other pattern recognition receptors may also be involved, and we could therefore have missed some alternative activation pathways.

We studied LPAR antagonism *in vitro* only, thus the multiple effects of LPAR antagonism need to be elucidated on animal models before applying these findings to individuals with ALF. Currently only LPAR1-3 antagonists are commercially available so more information could be gathered once it is possible for LPAR4-6 antagonism to be explored.

In individuals with ALF, LPCs are reduced and can be used as biomarkers of poor prognosis. The LPC-ATX-LPA axis modulates innate immune responses in ALF through LPAR1 and 3. LPA reduces the pro-restorative phenotypical markers MerTK and CD163 on monocytes and this can be reversed with LPAR antagonism. RNA sequencing unveiled further pathways linking lipid metabolism and immune dysfunction in ALF, distinct from LPAR expression. These preliminary findings highlight the importance of LPARs as possible therapeutic targets in ALF.

Affiliations

[1]Department of Inflammation Biology, School of Immunology and Microbial Sciences, Kings College London, UK; [2]Institute of Liver Studies, Kings College Hospital, Denmark Hill, London, UK; [3]Section of Hepatology and Gastroenterology, Department of Metabolism, Digestion and Reproduction, Faculty of Medicine, Imperial College, London, UK; [4]Oncology Safety, Clinical Pharmacology & Safety Sciences, R&D, Astra Zeneca, Cambridge, UK; [5]The Roger Williams Institute of Hepatology London, Foundation for Liver Research, London, UK; [6]Infection Clinical Academic group, St.George's University of London, UK; [7]Department of Biomedicine, University of Basel and University Centre for Gastrointestinal and Liver Diseases, Basel, Switzerland; [8]Anaesthetics, Critical Care, Emergency and Trauma Research Delivery Unit, Kings College Hospital, London, UK

Abbreviations

ACLF, acute on chronic liver failure; ALF, acute liver failure; ALI, acute liver injury; ATX, autotaxin; CTLA-4, cytotoxic T-lymphocyte-associated protein 4; HC, healthy control; LPA, lysophosphatidylcholinic acid; LPAR, LPA receptor; LPC, lysophosphatidylcholine; LPCAT, lysophosphatidylcholine acyltransferase; MELD, model of end-stage liver disease; MS, mass spectrometry; NK, natural killer; PBMCs, peripheral blood mononuclear cells; PC, phosphatidylcholine; PCA, principal component analysis; PD-1, programmed cell death 1; PD-L1, programmed cell death 1 ligand; PLA, phospholipase A; SOFA, Sequential Organ Failure Assessment.

Financial support

Biomedical Research Council at Guys and St Thomas NHS Foundation Trust; Kings Health Partners; Kings College Hospital Charity; Intensive Care Society UK; Medical Research Council; Imperial College London, Rosetrees Trust.

Conflict of interest

Muireann Coen is an employee of AstraZeneca and has stock ownership and/or stock options or interests in the company. William Bernal is consultant for Versantis AG and Pioneering Medicine VII, Inc.

Please refer to the accompanying ICMJE disclosure forms for further details.

Authors' contributions

FMT, MJWM, study concept and design; FMT, RZ, FA, SM, EJ, AC, MC, SN, AS, CB acquisition of data; FMT,MJWM, RZ, MC, IW, EH, PM, MC, RM, ET, SRA analysis and interpretation of data; FMT, MJWM, drafting of the manuscript; FMT, MJWM, MC, IW, JW, WB, KM, VCP, ET critical revision of the manuscript for important intellectual content; FMT, MJWM, RZ, SA statistical analysis; MJWM, VCP, KM, ET obtained funding; FMT, SN, SM, administrative, technical, or material support; MJWM, study supervision.

Data availability statement

Data can be made available at reasonable request and uploaded on acceptance.

Supplementary data

Supplementary data to this article can be found online at https://doi.org/10.1016/j.jhep.2022.10.031.

References

Author names in bold designate shared co-first authorship

[1] Trovato FM, Rabinowich L, McPhail MJW. Update on the management of acute liver failure. Curr Opin Crit Care 2019;25(2):157–164.

[2] Triantafyllou E, Woollard KJ, McPhail MJW, Antoniades CG, Possamai LA. The role of monocytes and macrophages in acute and acute-on-chronic liver failure. Front Immunol 2018;9:2948.

[3] Triantafyllou E, Gudd CL, Mawhin MA, Husbyn HC, Trovato FM, Siggins MK, et al. PD-1 blockade improves Kupffer cell bacterial clearance in acute liver injury. J Clin Invest 2021;131(4).

[4] Khamri W, Abeles RD, Hou TZ, Anderson AE, El-Masry A, Triantafyllou E, et al. Increased expression of cytotoxic T-lymphocyte-associated protein 4 by T cells, induced by B7 in sera, reduces adaptive immunity in patients with acute liver failure. Gastroenterology 2017;153(1):263–276 e8.

[5] Triantafyllou E, Pop OT, Possamai LA, Wilhelm A, Liaskou E, Singanayagam A, et al. MerTK expressing hepatic macrophages promote the resolution of inflammation in acute liver failure. Gut 2018;67(2):333–347.

[6] Antoniades CG, Khamri W, Abeles RD, Taams LS, Triantafyllou E, Possamai LA, et al. Secretory leukocyte protease inhibitor: a pivotal mediator of anti-inflammatory responses in acetaminophen-induced acute liver failure. Hepatology 2014;59(4):1564–1576.

[7] Jennings JJ, Mandaliya R, Nakshabandi A, Lewis JH. Hepatotoxicity induced by immune checkpoint inhibitors: a comprehensive review including current and alternative management strategies. Expert Opin Drug Metab Toxicol 2019;15(3):231–244.

[8] **Trovato FM**, **Zia R**, Napoli S, Wolfer K, Huang X, Morgan PE, et al. Dysregulation of the lysophosphatidylcholine/autotaxin/lysophosphatidic acid Axis in acute-on-chronic liver failure is associated with mortality and systemic inflammation by lysophosphatidic acid-dependent monocyte activation. Hepatology 2021;74(2):907–925. https://doi.org/10.1002/hep.31738.

[9] Beger RD, Bhattacharyya S, Yang X, Gill PS, Schnackenberg LK, Sun J, et al. Translational biomarkers of acetaminophen-induced acute liver injury. Arch Toxicol 2015;89(9):1497–1522.

[10] Liu W, Hopkins AM, Hou J. The development of modulators for lysophosphatidic acid receptors: a comprehensive review. Bioorg Chem 2021;117:105386.

[11] Schober A, Siess W. Lysophosphatidic acid in atherosclerotic diseases. Br J Pharmacol 2012;167(3):465–482.

[12] Yang L, Kraemer M, Fang XF, Angel PM, Drake RR, Morris AJ, et al. LPA receptor 4 deficiency attenuates experimental atherosclerosis. J Lipid Res 2019;60(5):972–980.

[13] Orosa B, Garcia S, Martinez P, Gonzalez A, Gomez-Reino JJ, Conde C. Lysophosphatidic acid receptor inhibition as a new multipronged treatment for rheumatoid arthritis. Ann Rheum Dis 2014;73(1):298–305.

[14] Miyabe Y, Miyabe C, Iwai Y, Takayasu A, Fukuda S, Yokoyama W, et al. Necessity of lysophosphatidic acid receptor 1 for development of arthritis. Arthritis Rheum 2013;65(8):2037–2047.

[15] Velasco M, O'Sullivan C, Sheridan GK. Lysophosphatidic acid receptors (LPARs): potential targets for the treatment of neuropathic pain. Neuropharmacology 2017;113(Pt B):608–617.

[16] Rancoule C, Pradere JP, Gonzalez J, Klein J, Valet P, Bascands JL, et al. Lysophosphatidic acid-1-receptor targeting agents for fibrosis. Expert Opin Investig Drugs 2011;20(5):657–667.

[17] Bae GH, Lee SK, Kim HS, Lee M, Lee HY, Bae YS. Lysophosphatidic acid protects against acetaminophen-induced acute liver injury. Exp Mol Med 2017;49(12):e407.

[18] Han MS, Park SY, Shinzawa K, Kim S, Chung KW, Lee JH, et al. Lysophosphatidylcholine as a death effector in the lipoapoptosis of hepatocytes. J Lipid Res 2008;49(1):84–97.

[19] Xu J, Casas-Ferreira AM, Ma Y, Sen A, Kim M, Proitsi P, et al. Lipidomics comparing DCD and DBD liver allografts uncovers lysophospholipids elevated in recipients undergoing early allograft dysfunction. Sci Rep 2015;5:17737.

[20] Cortes M, Pareja E, Garcia-Canaveras JC, Donato MT, Montero S, Mir J, et al. Metabolomics discloses donor liver biomarkers associated with early allograft dysfunction. J Hepatol 2014;61(3):564–574.

[21] Singer M, Deutschman CS, Seymour CW, Shankar-Hari M, Annane D, Bauer M, et al. The third international consensus definitions for sepsis and septic shock (Sepsis-3). JAMA 2016;315(8):801–810.

[22] Izzi-Engbeaya C, Comninos AN, Clarke SA, Jomard A, Yang L, Jones S, et al. The effects of kisspeptin on beta-cell function, serum metabolites and appetite in humans. Diabetes Obes Metab 2018;20(12):2800–2810.

[23] Trebicka J, Fernandez J, Papp M, Caraceni P, Laleman W, Gambino C, et al. The PREDICT study uncovers three clinical courses of acutely decompensated cirrhosis that have distinct pathophysiology. J Hepatol 2020;73(4):842–854.

[24] **McPhail MJW**, **Shawcross DL**, Lewis MR, Coltart I, Want EJ, Antoniades CG, et al. Multivariate metabotyping of plasma predicts survival in patients with decompensated cirrhosis. J Hepatol 2016;64(5):1058–1067.

[25] Ramaiah SK, Rittling S. Pathophysiological role of osteopontin in hepatic inflammation, toxicity, and cancer. Toxicol Sci 2008;103(1):4–13.

[26] Affo S, Dominguez M, Lozano JJ, Sancho-Bru P, Rodrigo-Torres D, Morales-Ibanez O, et al. Transcriptome analysis identifies TNF superfamily receptors as potential therapeutic targets in alcoholic hepatitis. Gut 2013;62(3):452–460.

[27] Ohradanova-Repic A, Machacek C, Charvet C, Lager F, Le Roux D, Platzer R, et al. Extracellular purine metabolism is the switchboard of immunosuppressive macrophages and a novel target to treat diseases with macrophage imbalances. Front Immunol 2018;9:852.
[28] Ancuta P, Liu KY, Misra V, Wacleche VS, Gosselin A, Zhou X, et al. Transcriptional profiling reveals developmental relationship and distinct biological functions of CD16+ and CD16- monocyte subsets. BMC Genomics 2009;10:403.
[29] Ma S, Xie Z, Zhang L, Yang Y, Jiang H, Ouyang X, et al. Identification of a potential miRNA-mRNA regulatory network associated with the prognosis of HBV-ACLF. Front Mol Biosci 2021;8:657631.
[30] Moore JK, MacKinnon AC, Man TY, Manning JR, Forbes SJ, Simpson KJ. Patients with the worst outcomes after paracetamol (acetaminophen)-induced liver failure have an early monocytopenia. Aliment Pharmacol Ther 2017;45(3):443–454.
[31] Rolando N, Wade J, Davalos M, Wendon J, Philpott-Howard J, Williams R. The systemic inflammatory response syndrome in acute liver failure. Hepatology 2000;32(4 Pt 1):734–739.
[32] Larsen FS, Schmidt LE, Bernsmeier C, Rasmussen A, Isoniemi H, Patel VC, et al. High-volume plasma exchange in patients with acute liver failure: an open randomised controlled trial. J Hepatol 2016;64(1):69–78.
[33] Srungaram P, Rule JA, Yuan HJ, Reimold A, Dahl B, Sanders C, et al. Plasma osteopontin in acute liver failure. Cytokine 2015;73(2):270–276.
[34] Riksen NP, Netea MG. Immunometabolic control of trained immunity. Mol Aspects Med 2021;77:100897.
[35] Knuplez E, Marsche G. An updated review of pro- and anti-inflammatory properties of plasma lysophosphatidylcholines in the vascular system. Int J Mol Sci 2020;21(12).
[36] Yung YC, Stoddard NC, Chun J. LPA receptor signaling: pharmacology, physiology, and pathophysiology. J Lipid Res 2014;55(7):1192–1214.
[37] Claria J, Curto A, Moreau R, Colsch B, Lopez-Vicario C, Lozano JJ, et al. Untargeted lipidomics uncovers lipid signatures that distinguish severe from moderate forms of acutely decompensated cirrhosis. J Hepatol 2021;75(5):1116–1127.
[38] Li J, Liang X, Jiang J, Yang L, Xin J, Shi D, et al. PBMC transcriptomics identifies immune-metabolism disorder during the development of HBV-ACLF. Gut 2022;71(1):163–175.
[39] Sun Y, Yu H, Li F, Lan L, He D, Zhao H, et al. Identification of hub genes and potential molecular mechanisms in patients with HBV-associated acute liver failure. Evol Bioinform Online 2020;16:1176934320943901.
[40] Zhao F, Hoechst B, Duffy A, Gamrekelashvili J, Fioravanti S, Manns MP, et al. S100A9 a new marker for monocytic human myeloid-derived suppressor cells. Immunology 2012;136(2):176–183.
[41] Kwak T, Wang F, Deng H, Condamine T, Kumar V, Perego M, et al. Distinct populations of immune-suppressive macrophages differentiate from monocytic myeloid-derived suppressor cells in cancer. Cell Rep 2020;33(13):108571.
[42] Bernsmeier C, Triantafyllou E, Brenig R, Lebosse FJ, Singanayagam A, Patel VC, et al. CD14(+) CD15(–) HLA-DR(–) myeloid-derived suppressor cells impair antimicrobial responses in patients with acute-on-chronic liver failure. Gut 2018;67(6):1155–1167.
[43] De la Cruz-Cano E. Association between FKBP5 and CRHR1 genes with suicidal behavior: a systematic review. Behav Brain Res 2017;317:46–61.
[44] Hojo Y, Ikeda U, Ohya K, Ichida M, Kario K, Takahashi M, et al. Interaction between monocytes and vascular endothelial cells induces adrenomedullin production. Atherosclerosis 2001;155(2):381–387.
[45] Kubo A, Minamino N, Isumi Y, Katafuchi T, Kangawa K, Dohi K, et al. Production of adrenomedullin in macrophage cell line and peritoneal macrophage. J Biol Chem 1998;273(27):16730–16738.
[46] Kohno M, Yokokawa K, Yasunari K, Minami M, Kano H, Hanehira T, et al. Induction by lysophosphatidylcholine, a major phospholipid component of atherogenic lipoproteins, of human coronary artery smooth muscle cell migration. Circulation 1998;98(4):353–359.
[47] Ajith Kumar AK. Adrenomedullin in sepsis: finally, a friend or an enemy? Indian J Crit Care Med 2020;24(12):1151–1153.
[48] Yan H, Jin S, Liang L, Du J, Aithal GP, Li L. Pro-adrenomedullin in acute decompensation of liver cirrhosis: relationship with acute-on-chronic liver failure and short-term survival. Scand J Gastroenterol 2020;55(5):606–614.
[49] Abate W, Alrammah H, Kiernan M, Tonks AJ, Jackson SK. Lysophosphatidylcholine acyltransferase 2 (LPCAT2) co-localises with TLR4 and regulates macrophage inflammatory gene expression in response to LPS. Sci Rep 2020;10(1):10355.
[50] Perez-Chacon G, Astudillo AM, Ruiperez V, Balboa MA, Balsinde J. Signaling role for lysophosphatidylcholine acyltransferase 3 in receptor-regulated arachidonic acid reacylation reactions in human monocytes. J Immunol 2010;184(2):1071–1078.
[51] Tang D, Chen X, Kang R, Kroemer G. Ferroptosis: molecular mechanisms and health implications. Cell Res 2021;31(2):107–125.
[52] Lee JY, Kim WK, Bae KH, Lee SC, Lee EW. Lipid metabolism and ferroptosis. Biology (Basel) 2021;10(3).
[53] Schmid B, Finnen MJ, Harwood JL, Jackson SK. Acylation of lysophosphatidylcholine plays a key role in the response of monocytes to lipopolysaccharide. Eur J Biochem 2003;270(13):2782–2788.
[54] Artru F, McPhail MJW, Triantafyllou E, Trovato FM. Lipids in liver failure syndromes: a focus on eicosanoids, specialized pro-resolving lipid mediators and lysophospholipids. Front Immunol 2022;13:867261.
[55] Zulfikar S, Mulholland S, Adamali H, Barratt SL. Inhibitors of the autotaxin-lysophosphatidic acid Axis and their potential in the treatment of interstitial lung disease: current perspectives. Clin Pharmacol 2020;12:97–108.
[56] Onorato JM, Shipkova P, Minnich A, Aubry AF, Easter J, Tymiak A. Challenges in accurate quantitation of lysophosphatidic acids in human biofluids. J Lipid Res 2014;55(8):1784–1796.

Journal of Hepatology, Volume ■

Supplemental information

Lysophosphatidylcholines modulate immunoregulatory checkpoints in peripheral monocytes and are associated with mortality in people with acute liver failure

Francesca M. Trovato, Rabiya Zia, Florent Artru, Salma Mujib, Ellen Jerome, Anna Cavazza, Muireann Coen, Ian Wilson, Elaine Holmes, Phillip Morgan, Arjuna Singanayagam, Christine Bernsmeier, Salvatore Napoli, William Bernal, Julia Wendon, Rosa Miquel, Krishna Menon, Vishal C. Patel, John Smith, Stephen R. Atkinson, Evangelos Triantafyllou, and Mark J.W. McPhail

Lysophosphatidylcholines modulate immunoregulatory checkpoints in peripheral monocytes and are associated with mortality in people with acute liver failure

Francesca M Trovato, Rabiya Zia, Florent Artru, Salma Mujib, Ellen Jerome, Anna Cavazza, Muireann Coen, Ian Wilson, Elaine Holmes, Phillip Morgan, Arjuna Singanayagam, Christine Bernsmeier, Salvatore Napoli, William Bernal, Julia Wendon, Rosa Miquel, Krishna Menon, Vishal C Patel, John Smith, Stephen R Atkinson, Evangelos Triantafyllou, Mark JW McPhail

Table of contents

Supplementary materials and methods

Isolation of PBMCs : Blood was diluted 1:1 v/v with phosphate buffer solution (PBS, Gibco™, Thermofisher, USA) in 50mL tube(s) and used to isolate PBMC by density gradient centrifugation using Ficoll-Paque Plus (GE Healthcare, UK) at 1:3 v/v?. Centrifuge: RCF 800xg for 20 min at room temperature with brake off. PBMCs were collected and resuspended with PBS and then centrifuged twice: RCF 800xg for 10min at room temperature with the brake on. The cell pellet was re-suspended in the desired volume according to following use destination, i.e., 1mL of complete medium for culture including RPMI 1640 medium (Gibco, Thermofisher USA)+ 10% Fetal Bovine Serum(FBS, Thermofisher) + 1% Penstrep (Penicillin-Streptomycin 10,000 U/mL, Gibco, Thermofisher, USA), or 500 µL of RPMI and transferred into 1ml cryovials containing 500 µL of freezing mix (20% Dimethylsulfoxide (DMSO) + 80% FBS to obtain a final concentration of 10% DMSO, 40% FBS, 50% medium), and then freeze/stored at -80°C for future phenotyping.

Isolation of plasma: Lithium heparin tubes were spun for 10 min at RCF 800xg (20°C) with brake on. Supernatants were transferred into 2 mL tubes and freeze/store at -80°C.

Proton nuclear magnetic resonance (^{1}H NMR) Spectroscopy

^{1}H NMR spectroscopy was initially used to profile plasma and identify the main metabolite groups perturbed in acute liver failure. Plasma ^{1}H NMR spectroscopic profiles were acquired using a 1-dimensional ^{1}H NMR pulse sequence (Carr Purcell-Meiboom-Gill (CPMG)).[1] Individual metabolites were identified by both comparing chemical shift values to published data and also identifying correlation patterns between specific peaks in the spectra. The correlation patterns were identified by performing statistical total correlation spectroscopy (STOCSY).[2]

All plasma samples were prepared according to the previously published paper by Dona et al[3]. Sample preparation and analysis order was orthogonal to the following metadata variables; 90-day survival score, disease group, age and gender. Following randomization, plasma samples (350 µl) were thawed and vortexed and centrifuged at 13,000 g for 5 minutes at 4 °C. Supernatant aliquots (300 µl) were added to 96 x 5 mm NMR tube SampleJet boxes, using a Bruker Sample Track system and a Liquid Handler 215 preparation robot. Phosphate buffer was also added to the 5mm NMR tubes (300 µl of 0.075 M NaH_2PO_4, 20% D_2O, pH 7.4, 2 mM NaN_3 and 4.6 mM TSP; 3-trimethyl-silyl-[2,2,3,3-2H4]-propionic acid, sodium salt 98 atom % D (Sigma-Aldrich, UK)). The tubes were sealed with POM balls (Bruker Biospin, Rheinstetten, Germany) and the samples thoroughly mixed by inverting the box and shaking multiple times. ^{1}H NMR spectra were acquired on a Bruker 600 MHz (Avance III) spectrometer, operating at a ^{1}H frequency of 600.16 MHz (14.1 Tesla) at 300K using a 5 mm BBI probe and an automated SampleJet system (Bruker Biospin, Rheinstetten, Germany). A one dimensional Carr Purcell-Meiboom-Gill (CPMG) spin echo sequence (d1-90°-(τ - 180°- τ)n-acquire) was used to attenuate the broader peaks arising from lipids and proteins. For each sample, 32 transients were collected into 73k data points using a spectral width of 20 ppm and a total spin echo time of 76.8 ms (τ of 300 µs, number of loops - 128). Suppression of the water signal was performed during the relaxation delay (d1 4s) and a line broadening function of 0.3 Hz was applied to all spectra prior to Fourier transformation.

^{1}H NMR spectral pre-processing was performed manually in TopSpin 3.0 NMR software (Bruker Biospin, Rheinstetten), where all spectra were Fourier transformed, phased, baseline corrected, and subsequently referenced to the α-glucose anomeric proton resonance at 5.23ppm. The digitised spectra (33k data points) were imported into Matlab (R2014a Mathworks, Natick, USA) and spectral regions exhibiting unwanted resonances were removed, for example, the water resonance region (δ 4.32 to 4.84 ppm). ^{1}H NMR data was mean centered and scaled to unit-variance prior to multivariate modelling which was performed using in-house scripts in Matlab.

Untargeted UPLC-MS Lipid analysis:

All mobile phases were prepared with LC−MS grade solvents: water (Fischer Scientific, New Jersey, USA), HPLC grade isopropanol (IPA), LC-MS grade acetonitrile (ACN), ammonium acetate, acetic acid and phosphoric acid (the latter all from Sigma-Aldrich (Dorset, U.K.)). The 12 lipid standard mix run was made up of LysoPC(9:0) (855276P), PC(11:0) (850399P), C(17:0) (H3500), PG(15:0) (840446P), PE(15:0) (840446P), PS(17:0) (840028P), PA(17:0) (830856P), Cer(17:0) (860517P), DG(19:0) (68633), PC(23:0) (850372P), TG(15:0) (T4257) and TG(17:0) (T2151) (Avanti Polar Lipids, Alabaster, Alabama) which are selected to be representative of each lipid class found in human blood, these have odd number fatty acid chains as they are less likely to overlap with endogenous lipids in the samples being analysed. Furthermore, lipid class mixtures which were analysed by subsequent MS/MS experiments were obtained from Avanti Polar Phospholipid mixes, which included soy PS mixture (870336), egg PG mixture (841138), egg PE mixture (841118), porcine brain ceramide mixture (860052P) and bovine milk SM mixture (860063). Fragmentation data from these lipid mixtures were used to aid metabolite identification of features from the sample by comparing to fragments obtained from known lipid classes.

Serum samples were thawed at 4°C and vortexed in batches according to plate number. An aliquot of 100µl per sample was added to each well of the lipid preparation and an additional 10µl per sample was aliquoted into a falcon tube to make up pooled QC. The pooled QC was added to the lipid preparation plate in column 12 at 100µl per well. In addition, 400µl of the 12 Lipid standard mix, dissolved in isopropanol (IPA), was added to each study and QC sample in the sample preparation plate. The lipid samples were prepared by protein precipitation using the IPA present in the lipid standard mix using an Eppendorf MixMate for 2 hours at 1400rpm at 4^{o}C, followed by centrifugation using RCF 3486 x g for 10 minutes at 4^{o}C. After centrifugation 125µl of the supernatant (organic phase) was added to the corresponding well of the analytical plate. For each lipid preparation plate three lipid analytical plates were prepared: two for analysis per ionisation mode (positive and negative) and one as a backup. The analytical plates were then heat-sealed using a heat seal foil, centrifuged at RCF 3486 x g for 5 minutes at 4^{o}C and stored at -80^{o}C until analysis. Furthermore, the pooled QC was aliquoted into seven tubes and diluted to make up a dilution series spanning seven points.). The remaining QC serum was separated into 175µl aliquots and placed into eppendorfs, to be used for conditioning of the UPLC-MS instrument. The lipid standard mix was added to both the dilution series and QC for conditioning prior to instrument set up, 700µl was added per 175µl of QC. All eppendorfs

were then centrifuged at 3486g for 10 minutes at 2-8^{o}C. The supernatant (organic phase) was taken and transferred into 300µl glass recovery vials and sealed with foil lined caps.

Ultra high performance liquid chromatography (UHPLC) was performed using an Acquity UPLC system (Waters Corp., USA) on a 2.1 × 100 mm Acquity UPLC BEH column containing a sub 2 µm C8 stationary phase. Sample injection volumes were 1 µl for +ve ESI and2 µl for -ve ESI respectively. The solvents used for UHPLC were H_2O/2-propanol/acetonitrile (2:1:1; v:v:v) containing 5 mM ammonium acetate, 0.05% acetic acid and 20 µM phosphoric acid as mobile phase A and isopropanol: acetonitrile (1:1; v:v) containing 5 mM ammonium acetate and 0.05% acetic acid as mobile phase B. These solvents were delivered at a flow rate of 0.6 ml/min with the starting condition for the gradient set at 1% mobile phase B for 0.1 min. thereafter the composition of the solvent changed to 30% mobile phase B over the period 0.1 to 2 min followed by a further linear increase to 90% mobile phase B at 11.5 min. At 12 min the solvent composition was raised to 99.99% mobile phase B and held there until 12.55 min before returning to the initial condition for re-equilibration prior to the next injection (the run time was 15 min/sample)

Lipids were detected via MS on a Xevo G2-S QToF MS instrument (Waters MS Technologies, UK) using both +ve and -ve electrospray ionisation (ESI). MS was performed with a capillary voltage of 2.0 kV (+ve ESI) or 1.5 kV (-ve ESI)f with the sample cone voltage set to 25 V, the source offset at 80, and a source temperature of 120 °C. The desolvation temperature was 600 °C with the desolvation gas and cone gas flows at 1000 and 150 L/h repectively. MS data were acquired in centroid mode over the scan range 50–2000 m/z using a scan time of 0.1 s. The lockSpray mass correction, used to ensure mass accuracy was achieved using leucine enkephaline (m/z 556.2771 in +ve ESI and 554.2615 in -ve ESI) at a 600 pg/ µL dissolved in H_2O/ACN solution (50:50; v/v) delivered at 15 µl/min.

The Waters raw data files were converted to the netCDF format using the Databridge tool provided in the MassLynx 4.1 software (Waters, Milford, USA) Peak picking was then performed using the XCMS package implemented in R (v.3.2.5 using RStudio v.0.99.482). The centWave algorithm was used for peak picking, while the peak grouping step was performed with the density method. After obtaining a final feature list with XCMS, the data sets were then ran through the nPYc-Toolbox pipeline for MS data quality control, feature filtering and batch correction. Batch effect correction was performed by applying the LOESS based correction available in the nPYc-Toolbox. Briefly, for each feature a LOESS smoothing curve is fitted to the intensity values detected in the QC samples, and the LOESS fit is then interpolated to cover the whole run order. Each sample is then divided by the value estimated in the LOESS curve. Features where negative or 0 values were obtained (typically caused by very low intensity features) were removed, as no batch correction is possible in that case. Whenever there are multiple separate batches (caused by stoppages in the data acquisition, for example), a separate LOESS curve is estimated for each batch. These are then corrected individually using their respective LOESS fits, and then each batch is aligned to the median of the batch medians. The LOESS window parameter was set to 11, the default value in the nPYc-Toolbox (meaning that the LOESS fit at each point is estimated from the adjacent 11 samples).

As part of the feature filtering process, all features whose relative standard deviation (RSD) calculated on the study samples was smaller than the one measured on the QC samples or whose RSD estimated from the latter was greater than 30% were removed Features whose Pearson correlation with dilution estimated in the dilution series was lower than 0.7 were also removed. XCMS parameters were selected by manual analysis of the data.

UPLCMS - BIOCRATES p180 assay:

We utilised the AbsoluteIDQ® p180 kit (Biocrates Life Sciences, Austria) which is a fully automated assay based on phenylisothiocyanate (PITC) derivatization of the target analytes using internal standards for quantification. Amino acids and biogenic amines were determined in LC-MS mode, acylcarnitines, phospholipids (lyso-phosphatidylcholines with acyl residue at CXX:X, phosphatidylcholine with diacyl residue sum CXX:X (PC aa), and phosphatidylcholine with acyl-alkyl residue sum CXX:X (PC ae)), sphingomyelins, and the sum of hexoses were analysed using flow injection analysis (FIA). Heparin plasma samples were prepared according to the manufacturers protocols.
Briefly, 10 µL of internal standard followed by 10 µL of sample (plasma after centrifugation at 4°C for 5 min at 2750 x g), calibrator or quality controls (QC), were transferred onto the filter located in the wells of the upper 96-well plate and dried for 30 min under a nitrogen stream. Thereafter, 50 µL of a 5% phenylisothiocyanate (PITC, Sigma-Aldrich, UK) solution (in ethanol:water:pyridine, 1:1:1 (v/v)) was added to derivatize amino acids and biogenic amines. After 20 min incubation, the filter spots were dried again for 60 min before the metabolites were extracted using 5 mM ammonium acetate in methanol (300 µL). After shaking (450 rpm, 30 min), the eluate was collected into the lower 96-well plate by centrifugation (500 x g, 2 min).

150 µL of extract were transferred to an empty 96-deep-well plate and diluted with 150 µL of water, and the plate sealed. After shaking (600 rpm, 2 min) the plate was transferred for analysis by liquid chromatography-tandem mass spectrometry (LC-MS/MS).

For flow injection analysis (FIA)-mass spectrometry, 20 µL of the original, undiluted extract were transferred to a separate 96-deep-well plate, and diluted with 380 µL FIA mobile phase, sealed and shaken (600 rpm, 2 min). A Xevo Acquity TQ-S micro (Waters Corp., MA, US) instrument at King's College Hospital was used for both LC and FIA analysis of the samples. Separation (LC) was achieved using a BEH-C18 UPLC column (75 mm x 2.1 mm i.d., Waters Corp., MA, US), with all mobile phases and instrument settings according to the Biocrates protocol. The ratio of analyte to internal standard was used for quantification purposes.

Cytokine analysis:

V-PLEX Proinflammatory Panel 1 Human Kit (IFN-γ, IL-1β, IL-2, IL-4, IL-6, IL-8, IL-10, IL-12p70, IL-13, TNF-α) from Meso Scale Diagnostics, LLC

Heparin plasma samples were 2-fold diluted. 50 µL of calibrators or sample were added to each well of a V-PLEX plate and incubated for 2 hours on a horizontal orbital microplate shaker at room temperature. Plates were then washed three times (20-fold wash buffer concentrate reconstituted). 25 µL of detection antibody solution were added to each well and incubated for 2 hours on a horizontal orbital microplate shaker at room temperature. 150 µL of a 2X Read Buffer T were added to each well and the plate was read with a MSD instrument. Average of the duplicate readings for each standard and sample were analysed and analyte concentrations established fitting a 4-parameter logistic calibration curve.

Enzyme linked immuno- absorbent assay (ELISA) techniques

ELISA kits for M65 and M30 (total and caspase-cleaved cytokeratin-18; Peviva, West Chester, OH), ATX/ENPP2 (R&D Systems, Minneapolis, USA), PLA_1 (Elabscience, Wuhan, China), PLA_2 (Biomatik, USA), general LPA (ABclonal Biotechnology Co., USA), Osteopontin (OPN, Biotechne, Minneapolis, USA), were obtained and serum/plasma concentrations quantified according to the manufacturer's instructions briefly summarised below.

M30 Apoptosense Elisa kit from PEVIVA

Heparin plasma samples were used. 25 µL Of standard or sample were added to each well of a precoated microplate together with 75 µL of diluted M30 Conjugate solution. After 4 hours incubation at room temperature on a horizontal orbital microplate shaker set at 600 rpm, plates were washed three times (reconstituted wash tablet solution). 200 µL of TMB Substrate Solution were added in each well and plates were incubated for 20 minutes at room temperature, protected from light. The reaction was stopped with 50 µL of Stop Solution per well. Optical density was assessed soon after, using a FLUOstar® Omega microplate reader (BMG Labtech Ltd, UK) set to 450 nm with 540 nm wavelength correction. Average of the duplicate readings for each standard and sample were analysed after subtraction of the average zero standard optical density. A third order polynomial standard curve was used for quantification.

ATX - Quantikine®ELISA Human ENPP-2/Autotaxin Immunoassay from R&D Systems

Heparin plasma samples were diluted 20-fold. 100 µL Of Assay Diluent RD1-34 were added to each well of a precoated microplate together with 50 µL of standard or sample. After 2 hours incubation at room temperature on a horizontal orbital microplate shaker (0.12" orbit) set at 500 ± 50 rpm, plates were washed three times (25- fold wash buffer concentrate reconstituted). 200 µL Of Human ENPP-2 Conjugate were added to each well and after 2 hours incubation at room temperature on the shaker, plates were washed three times. Then, 200 µL of Substrate Solution per well were added and plates were incubated for 30 minutes at room temperature, protected from light. The reaction was stopped with 50 µL of Stop Solution per well. Optical density was assessed soon after, using a FLUOstar® Omega microplate reader (BMG Labtech Ltd, UK) set to 450 nm with 540 nm wavelength correction. Average of the duplicate readings for each standard, control, and sample were analysed after subtraction of the average zero standard optical density. A third order polynomial standard curve was used for quantification

the data.

PLA1 - Human PLA1(Phospholipase A1) ELISA Kit from Elabscience Biotechnology Inc

Heparin plasma samples were 50-fold diluted. 100 µL Of standard or sample were added to each well of a precoated plate and incubated for 90 minutes at 37°. After samples removal, without washing, 100 µL of Biontinylated detection Ab working solution were added to each well and incubated at 37° for 1 hour. Plates were then washed three times (25- fold wash buffer concentrate reconstituted) . 100 µL Of HRP Conjugate working solution were added to each well and incubated at 37° for 30 mins, then plates were washed three times. 90 µL Of Substrate Reagent were added to each well and plates were incubated at 37° for 15 mins protected from light. The reaction was stopped with 50 µL of Stop Solution per well. Optical density was assessed soon after, using a FLUOstar® Omega microplate reader (BMG Labtech Ltd, UK) set to 450 nm. Average of the duplicate readings for each standard and sample were analysed after subtraction of the average zero standard optical density. A third order polynomial standard curve was used for quantification

PLA2 - Human Phospholipidase A2, PLA2 ELISA Kit from Biomatik

Heparin plasma samples were 10-fold diluted. 100 µL Of standard or sample were added to each well of a precoated plate and incubated for 2 hours at 37°. After samples removal, without washing, 100 µL Of Biontin-Antibody (1x) were added to each well and incubated at 37° for 1 hour. Plates were then washed three times (25-fold wash buffer concentrate reconstituted). 100 µL Of HRP- avidin (1x) solution were added to each well and incubated at 37° for 1 hour, then plates were washed three times. 90 µL Of TMB Substrate were added to each well and plates were incubated at 37° for 20 mins protected from light. The reaction was stopped with 50 µL of Stop Solution per well. Optical density was assessed soon after, using a FLUOstar® Omega microplate reader (BMG Labtech Ltd, UK) set to 450 nm with 540 nm wavelength correction. Average of the duplicate readings for each standard and sample were analysed after subtraction of the average zero standard optical density. A third order polynomial standard curve was used for quantification.

Total LPA – General Lysophosphatidic Acid ELISA Kit (LPA) from ABclonal Biotechnology

Heparin plasma samples were used. 50 µL Of standard or sample were added to each well of a precoated plate together with 50 µL of Biotin Conjugate Antigen Working Solution and incubated for 1 hour at 37°. After samples removal, plates were then washed three times (30-fold wash buffer concentrate reconstituted). 100 µL Of Streptavidin-HRP Working Solution were added to each well and incubated at 37° for 30 minutes, then plates were washed three times. 90 µL of TMB Substrate were added to each well and plates were incubated at 37° for 20 mins protected from light. The reaction was stopped with 50 µL of Stop Solution per well. Optical density was assessed soon after, using a FLUOstar® Omega microplate reader (BMG Labtech Ltd, UK) set to 450 nm with 570 nm wavelength correction. Average of the duplicate readings for each standard and sample were analysed after subtraction of the average zero standard optical density. A third order polynomial standard curve was used for quantification the data.

Human Osteopontin (OPN) ELISA kit from Bio-Techne

Heparin plasma samples were 300-fold diluted. 100 µL Of standard or sample were added to each well of a plate previously coated with Mouse Anti-Human Osteopontin Capture Antibody and kept overnight at room temperature. After 2 hours incubation at room temperature on a horizontal orbital microplate shaker (0.12" orbit) set at 500 ± 50 rpm, plates were washed three times (wash buffer: 0.05% Tween® 20 in PBS). 100 µL Of Biotinylated Goat Anti-Human Osteopontin Detection Antibody was added to each well and after 2 hours incubation at room temperature on the shaker, plates were washed three times. Then, 100 µL of Streptavidin-HRP were added and incubated for 20 mins avoiding light. After washing, 100 µL Of Substrate Solution (10mg *O*-phenylenediamine dihydrochioride in 25 ml of 0.05M phosphate citrate buffer) per well was added and plates were incubated for 20 minutes at room temperature, protected from light. The reaction was stopped with 50 µL of Stop Solution (2N H2SO4) per well. Optical density was assessed soon after, using a FLUOstar® Omega microplate reader (BMG Labtech Ltd, UK) set to 490 nm. The mean of the duplicate readings for each standard, control, and sample were analysed after subtraction of the average zero standard optical density. A third order polynomial standard curve was used for quantification.

Interleukin (IL) 6 in cell culture supernatants - Human IL-6 DuoSet ELISA kit from R&D Systems

Cell culture supernatant samples were 4-fold diluted. Plated were coated the day before the experiment with 100 µL of Capture Antibody at working concentration. After overnight incubation and three time washing (0.05% Tween 20 in PBS), 300 µL of Reagent Diluent were added per well and plates were incubated for 1 h. After washing, 100 µL of standard or sample were added to each well. After 2 hours incubation at room temperature on a horizontal orbital microplate shaker (0.12" orbit) set at 500 ± 50 rpm, plates were washed three times. 100 µL of Detection Antibody, diluted in Reagent Diluent, were added to each well and after 2 hours incubation at room temperature on the shaker, plates were again washed three times. Then, 100 µL of Streptavidin-HRP at working solution were added and plates were incubated for 20 minutes at room temperature, protected from light. After washing, 100 µL of Substrate Solution were added to each well, and incubated for further 20 minutes, protected from light. The reaction was stopped with 50 µL of Stop Solution per well. Optical density was assessed soon after, using a FLUOstar® Omega microplate reader (BMG Labtech Ltd, UK) set to 450 nm with 540 nm wavelength correction. Average of the duplicate readings for each standard, control, and sample were analysed after subtraction of the average zero standard optical density. A third order polynomial standard curve was used for quantification.

Single-epitope enzymatic immunohistochemistry for detection of ATX-positive cells.

Formalin-fixed paraffin embedded (FFPE) liver tissue was cut at 4 µm using a Leica RM2235 rotary microtome (Leica Biosystems, UK) and picked up on poly-L-lysine coated slides. Slides were dewaxed in xylene (5min - twice), rehydrated (100%, 90% and 70% ethanol - 5min each), bathed in sodium citrate buffer (pH6) and subjected to heat-induced epitope retrieval (HIER) for 20 min using a microwave. Slides were next rinsed in tapped water, allowed to cool down, incubated with protein block (10min) and dual-endogenous enzyme block (5min) (Agilent Technologies, UK), followed by 1.5 hour incubation

(room temperature) with primary antibody ENPP2 (Abcam # ab77104, UK). Signal was detected using the EnVision™ G|2 doublestain system – rabbit/mouse (DAB+/permanent red) detection kit (Agilent Technologies, UK), as per manufacturer's instructions. After hematoxylin counterstaining, slides were dehydrated (70%, 90% and 100% ethanol - 3min each), cleared with xylene (3min – twice) and cover-slipped with DPX mounting medium (Leica Biosystems, UK). Images were captured with a Nikon Eclipse E600 microscope using the Nuance™ 3.0.2 (PerkinElmer, UK) multispectral imaging technology

Cell Culture

Isolated PBMCs from both HC and ALF patients were incubated at 37°C, 5% CO_2 in a 24 well plate (0.5 x 10^6 cells per well) for 24 hours in 1 ml of complete medium (RPMI without HEPES, 10% FBS, 1% Antibiotic Antimycotic Solution). Different lipids (LPA 16:0, LPA 18:0, LPA 18:1, LPC 16:0, LPC 18:0 - Avanti Polar Lipids, Alabaster, AL) were added after 1h of culture: 1 µL of a 30 mM stock solution per well to reach 30 µM final concentration. After incubation, cells were washed with PBS and stained for phenotyping as follows. Supernatant was used for cytokine assays.

Antagonists and agonist culture

Isolated PBMCs were incubated at 37°C, 5% CO_2 in a 24 well plate (0.5 x 10^6 cells per well) for 20 hours in 1 ml of complete medium (RPMI without HEPES, 10% FBS, 1% Antibiotic Antimycotic Solution) with H2L5186303 (Sigma-Aldrich), Ro 6842262(Bio-techne) or Ki 16425(Sima-Aldrich). LPA16:0 (30µM), was added 30 mins after addition of the antagonist. The optimal concentration of antagonist was evaluated testing 0.001µM, 0.01 µM,1µM and 10 µM on cells from both HC and ALF (data not shown). The concentration of 1µM was found the most effective in modulating monocyte phenotype and thus used for the following experiments.

Immunophenotyping

Monocyte phenotype was determined by flow cytometry on fresh/cultured PBMCs using monoclonal antibodies against CD (Cluster of differentiation)14, CD16, CD163, chemokine receptor (CCR) 2 (Biolegend, USA), Human Leukocyte Antigen - DR isotype (HLA-DR) (eBioscience), Mer-Tyrosine Kinase (TK) (R&D Systems, USA), Programmed death-ligand 1 (PD-L1) (Biolegend, USA), Programmed cell death protein-1 (PD-1) (BD) and Fixable Viability Dye eFluor 506 (Invitrogen). For T cells phenotype CD3, CD8, T cell immunoreceptor with Ig and ITIM domains (TIGIT), Cytotoxic T-Lymphocyte Antigen 4 (CTLA-4), (eBioscience), PD-L1, T cell immunoglobulin and mucin domain-containing protein 3 (Tim-3), CD4, CD45, CD56 (Biolegend, USA), CD25, PD-1 (BD), CD127 and Fixable Viability Dye eFluor 506 (Invitrogen) were used (Antibody details can be found in **Table 3**).

Results are expressed as percentage (%) and/or mean fluorescence intensity (MFI). The acquisition was performed on a BD LSRFortessa™ cell analyzer (BD Biosciences). Flow cytometry data analysis was performed in FlowJo™ v10 (Becton Dickinson & Company).

Monocyte total RNA isolation

Monocytes were isolated by positive selection using CD14 MicroBeads (Miltenyi Biotec) according to manufacturer's instructions. Briefly, PBMCs were resuspended and passed through 30µm nylon mesh (#130-041-407) for single-cell suspension and centrifuged at 1800RPM for 5 min. After supernatant removal every 10^7 cells were resuspended in 80 µl of buffer + 20 µl of CD14 Microbeads and incubated for 15 min at 4°, then washed, centrifuged and resuspended in 500 µl buffer consisting of MACS BSA Stock solution (#130-091-376) diluted 1:20 with autoMACS Rinsing solution (#130-091-222). Magnetic separation was done with LS columns. Cell suspension was added to the column and washed 3 times with 3 ml of buffer. The column was then removed from the separator and placed into a collection tube (CD14+ cells tube). 5 ml of buffer was pipetted into the column and magnetically labelled cells were flushed into a new tube by firmly pushing the plunger. Cell pellet was resuspended in 100 µL RNA Lysis Solution and stored at -80.

The Ambion® RNAqueous®-Micro Kit (#AM1931) was then used to isolate total RNA according to manufacturer's instruction. Briefly, 50 µL of 100% ethanol, was added to the RNA lysate. The solution was loaded onto a Micro Filter Cartridge Assembly and centrifuged for ~30 sec at maximum speed. 180 µL of Wash Solution 1 was added to the filter and centrifuged for ~30 sec to pass the solution through the filter. This step was repeated twice using 180 µL of Wash Solution 2/3. The flow-through was then removed and the tube was again centrifuged for 1 minute at maximum speed.

The Micro Filter Cartridge was then transferred into a Micro Elution Tube. 10 µL of Elution Solution, preheated to 75°C, was added to the center of the filter and stored for 1 min at room temperature. Then the assembly was centrifuged for ~1min to elute the RNA from the filter. The step was repeated twice, adding other 10 µL of preheated Elution Solution, and collecting the eluate in the same Micro Elution Tube. Then we proceeded to the DNase I Treatment and DNase Inactivation. 10x DNAse buffer was added 1/10 to the sample together with 1 µL of DNAse I and incubated for 20 mins at 37oC. 2 µL of DNase Inactivation Reagent was added and stored for 2 mins at room temperature after vortexing. The mixture was then centrifuged for 1.5 min at maximum speed to pellet the DNase Inactivation Reagent. Extracted RNA was checked for sufficient quantity (Nanodrop A280, ThermoFisher, Wilmington, USA) (amount of >400ng, volume of >20ul and concentration of >20ng/ul) and quality (RIN > 8; Bioanalyzer 2100, Agilent, Santa Clara, USA). RNA was transferred to a fresh RNase-free tube and stored at –80°C. Samples were then shipped to Novogene (China) for RNA sequencing.

RNA sequencing

Library preparation was performed using NEBNext Ultra RNA Library Prep Kit for Illumina (New England BioLabs, Ipswich, USA). A 250~300 bp insert strand specific library was built up with rRNA removal method with TruSeq Stranded Total RNA Library Prep for rRNA removal and Novogene NGS Stranded RNA Library Prep Set (PT044) for library preparation, as follows:

Firstly, ribosomal RNA was removed by rRNA removal kit, and rRNA free residue was cleaned up by ethanol precipitation. Subsequently, sequencing libraries were generated using the rRNA-depleted RNA. After fragmentation, the first strand cDNA was synthesized using random hexamer primers. Then the second strand cDNA was synthesized, and deoxyuridine triphosphates (dUTPs) were replaced with

Deoxythymidine triphosphates (dTTPs) in the reaction buffer. The directional library was ready after end repair, A-tailing, adapter ligation, size selection, USER enzyme digestion, amplification, and purification. The insert size of the library was validated on a Bioanalyzer 2100 (Agilent, Santa Clara, USA) and quantified by PCR. Libraries were sequenced on Illumina NovaSeq 6000 S4 flowcell (Illumina, San Diego, USA) using 150bp paired-end reads to a target sequencing depth of 40 million read pairs per sample. Sequence data were evaluated for quality control issues using fastqc v0.11.9 (Available online at: http://www.bioinformatics.babraham.ac.uk/projects/fastqc/). Adaptors were trimmed using trimgalore v0.6.5 (https://github.com/FelixKrueger/TrimGalore). Reads were aligned to reference genome GRCh38[4] and corresponding Ensembl genebuild release 104 using the STAR 2.7.9a aligner[5]. Transcript quantification was performed using the RSEM 1.3.3 algorithm[6]. Raw count data were analysed in R v4.0.4 (R Statisical Foundation, Vienna, Austria). Differential expression analyses were conducted using the limma-voom pipeline (limma v3.46.0)[7]. Lowly expressed genes were filtered; count data were normalised and transformed and associated precision weights generated using the voom() function. Count data were modelled using a design model incorporating clinical group, blocked on batch and without an intercept (~0+Group+Batch); differential gene expression was estimated for contrasts of interest. Pathway analysis was conducted using Generally Applicable Gene-set Enrichment for Pathway Analysis (GAGE, gage v2.40.2)[8] and human KEGG pathways (release 103.0) annotated as "signalling" or "metabolism". Due to the exploratory nature of the analysis unadjusted p-values were used and a=0.05 used as the threshold to define significance.

Statistical Analysis

For ^{1}H NMR spectroscopic and UPLC-MS data, principal components analysis (PCA) was performed to visualise any inherent clustering and identify outliers (SIMCA v 16:0). Orthogonal projection to latent structure (OPLS) analysis was performed to maximise modelling of class differences while minimising variability unrelated to class. The R^2 value was calculated to give a measure of the goodness-of-fit or amount of variability explained by the model. A cross-validated Q^2 statistic (leave-one-out algorithm) was calculated as a quantitative measure of the predictability of the model for the Y variable. The cross-validated analysis of-variance (CV-ANOVA) statistic corresponds to a null-hypothesis of equal predictive residuals. Sensitivity and specificity were calculated from the cross validated Y-predicted variable. The S-plot loadings (displaying correlation versus covariance of spectral variables) and the variable importance in projection (VIP) plot were used to determine the metabolites contributing to class separation for UPLC-MS data. AUROC comparison was by the Hanley-McNeill method. T-test, one-way ANOVA/Kruskal-Wallis, Pearson/Spearman's correlations and AUROC were calculated with GraphPad Prism v 8.2.1 (GraphPad Software, San Diego, CA). Metabolite pathway and quantitative metabolite enrichment analyses were performed in metaboanalyst[9] (http://www.metaboanalyst.ca/) and

used metabolite information from the KEGG database[10] (https://www.genome.jp/kegg/). Public microarray datasets (Gene Expression Omnibus dataset series GSE16836, GSE61298, GSE80751) were interrogated to measure selected genes of interest in liver tissue. QIAGEN Ingenuity Pathway Analysis (QIAGEN IPA) was used to explore the pathway of interest. For the RNA sequencing analysis please see the previous section.

Sample size calculation: As per our previous work in ACLF for a lipid biomarker to have adequate discrimination between patients with ALF who survived or died we would need 36 patients (assuming lipid concentration in the SS of 16 arb units, 8 arb units in the group who died, assumed average standard deviation of 12 arb units and with a power of 80% and alpha of 0.05.

Supplementary figures

Fig. S1. Lysophospholipids are crucial in acute liver failure and related to the severity of the disease and the inflammation status

A,B,C): From enrichment analysis, phospholipids biosynthesis is the principal pathway differentiating ALF from HC (A) and cirrhosis (B) but not from Sepsis (C).p value according to the colour bar, red e^{-23} to yellow e^{-03}.

D&E) LPC 16:0 and 18:0 are directly correlated with lymphocyte count, IL-10, IL-6 ,IL-8 and IL-1B and inversely with monocyte and neutrophil counts t, Correlation matrix, Spearman's Correlation, correlation coefficients (rho) are showed per each pair in the corresponding cell. (E) All tree lipids (LPC 16:0, LPC 18:0, LPC 18:1) are inversely with MELD in ALF. Pearson's Correlation r and p are shown. Level of significance: LPC 16:0 *p=0.232, LPC 18:0 p=0.0794, LPC 18:1 *p=0.0346.

F) No difference was found in LPCs levels according to organ failures (renal, circulatory, respiratory). RRT= renal replacement therapy, Vasopr=vasopressors requirements, P/F= PaO2/FiO2. Mann-Whitney test used. All the comparisons were not statistically significant, only in the high P/F group, LPC 16:0 was increased in sepsis compared to ALF p*=0.0314

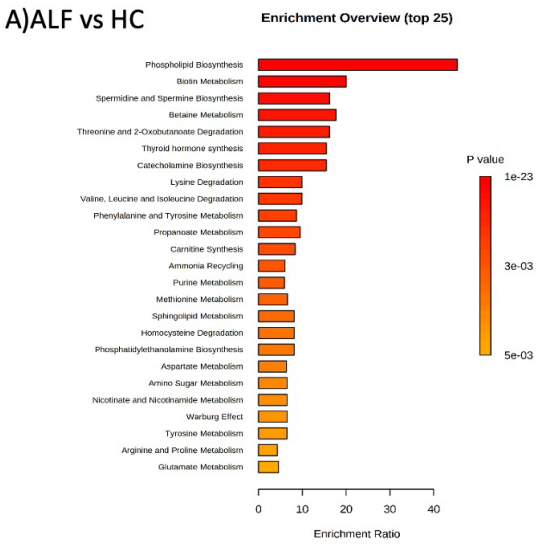
A)ALF vs HC
Enrichment Overview (top 25)
Phospholipid Biosynthesis
Biotin Metabolism
Spermidine and Spermine Biosynthesis
Betaine Metabolism
Threonine and 2-Oxobutanoate Degradation
Thyroid hormone synthesis
Catecholamine Biosynthesis
Lysine Degradation
Valine, Leucine and Isoleucine Degradation
Phenylalanine and Tyrosine Metabolism
Propanoate Metabolism
Carnitine Synthesis
Ammonia Recycling
Purine Metabolism
Methionine Metabolism
Sphingolipid Metabolism
Homocysteine Degradation
Phosphatidylethanolamine Biosynthesis
Aspartate Metabolism
Amino Sugar Metabolism
Nicotinate and Nicotinamide Metabolism
Warburg Effect
Tyrosine Metabolism
Arginine and Proline Metabolism
Glutamate Metabolism
P value
1e-23
3e-03
5e-03
0
10
20
30
40
Enrichment Ratio

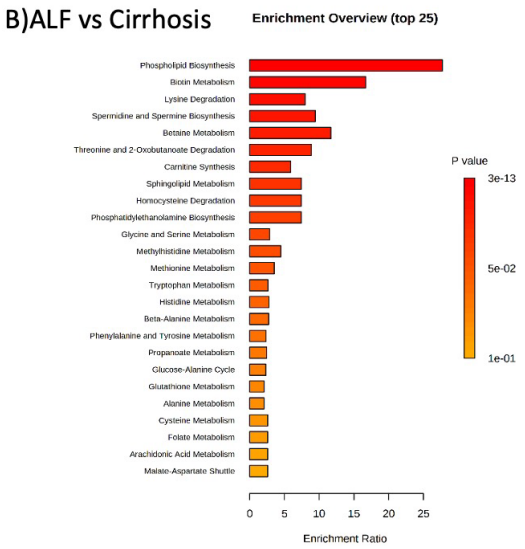
B)ALF vs Cirrhosis
Enrichment Overview (top 25)
Phospholipid Biosynthesis
Biotin Metabolism
Lysine Degradation
Spermidine and Spermine Biosynthesis
Betaine Metabolism
Threonine and 2-Oxobutanoate Degradation
Carnitine Synthesis
Sphingolipid Metabolism
Homocysteine Degradation
Phosphatidylethanolamine Biosynthesis
Glycine and Serine Metabolism
Methylhistidine Metabolism
Methionine Metabolism
Tryptophan Metabolism
Histidine Metabolism
Beta-Alanine Metabolism
Phenylalanine and Tyrosine Metabolism
Propanoate Metabolism
Glucose-Alanine Cycle
Glutathione Metabolism
Alanine Metabolism
Cysteine Metabolism
Folate Metabolism
Arachidonic Acid Metabolism
Malate-Aspartate Shuttle
P value
3e-13
5e-02
1e-01
0
5
10
15
20
25
Enrichment Ratio

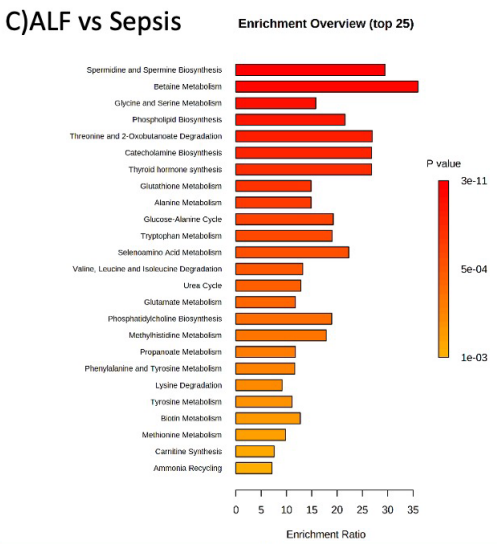
C)ALF vs Sepsis
Enrichment Overview (top 25)
Spermidine and Spermine Biosynthesis
Betaine Metabolism
Glycine and Serine Metabolism
Phospholipid Biosynthesis
Threonine and 2-Oxobutanoate Degradation
Catecholamine Biosynthesis
Thyroid hormone synthesis
Glutathione Metabolism
Alanine Metabolism
Glucose-Alanine Cycle
Tryptophan Metabolism
Selenoamino Acid Metabolism
Valine, Leucine and Isoleucine Degradation
Urea Cycle
Glutamate Metabolism
Phosphatidylcholine Biosynthesis
Methylhistidine Metabolism
Propanoate Metabolism
Phenylalanine and Tyrosine Metabolism
Lysine Degradation
Tyrosine Metabolism
Biotin Metabolism
Methionine Metabolism
Carnitine Synthesis
Ammonia Recycling
P value
3e-11
5e-04
1e-03
0
5
10
15
20
25
30
35
Enrichment Ratio

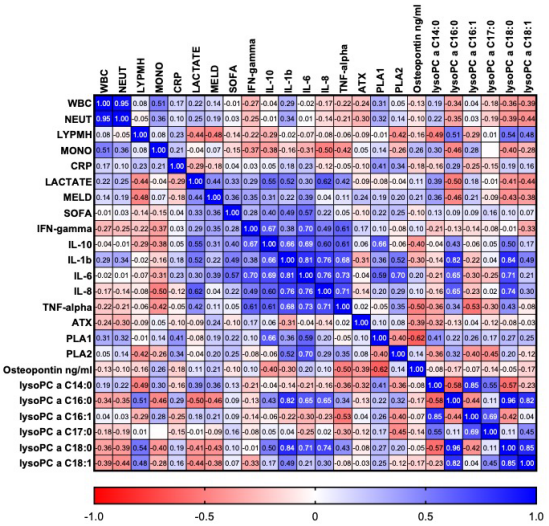
D)
WBC
NEUT
LYPMH
MONO
CRP
LACTATE
MELD
SOFA
IFN-gamma
IL-10
IL-1b
IL-6
IL-8
TNF-alpha
ATX
PLA1
PLA2
Osteopontin ng/ml
lysoPC a C14:0
lysoPC a C16:0
lysoPC a C16:1
lysoPC a C17:0
lysoPC a C18:0
lysoPC a C18:1
-1.0
-0.5
0
0.5
1.0

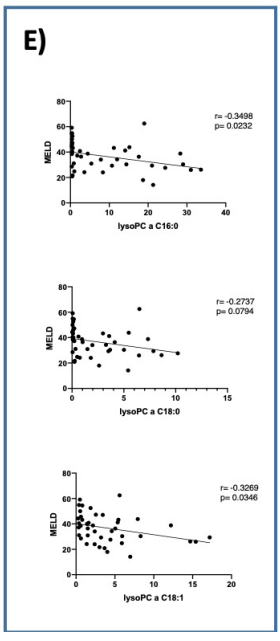
E)
r= -0.3498
p= 0.0232
MELD
lysoPC a C16:0
r= -0.2737
p= 0.0794
MELD
lysoPC a C18:0
r= -0.3269
p= 0.0346
MELD
lysoPC a C18:1

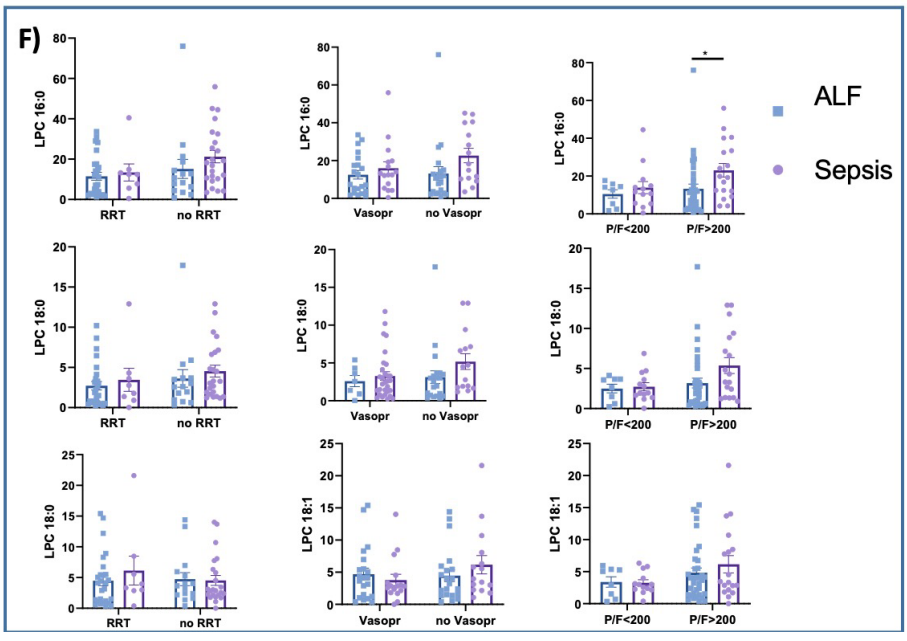
F)
LPC 16:0
LPC 18:0
LPC 18:1
RRT
no RRT
Vasopr
no Vasopr
P/F<200
P/F>200
*
ALF
Sepsis

Fig. S2. Immunohistochemistry showed ATX expression in viable hepatocyte in acute liver failure

A) Acute liver failure secondary to HELLP (Hemolysis, Elevated Liver enzymes and Low Platelets) syndrome, explanted liver.

ENPP2/ATX expression is observed in areas of viable hepatocytes (*). Large irregular areas of hepatocellular loss are observed at the left and bottom side of the picture (dotted line demarcates the area of necrosis). PT = portal tract, CV= central venule (40X)

B) Detail of a portal area with viable periportal hepatocytes (200X)

C) Acute liver failure secondary to paracetamol overdose, explanted liver.

ENPP2/ATX expression is observed in viable hepatocytes (*) in a liver with extensive multiacinar collapse post-necrosis (left side of the picture). PT= portal tract, CV= central venule, (40X).

D) Detail of a portal area with viable periportal hepatocytes, (200X).

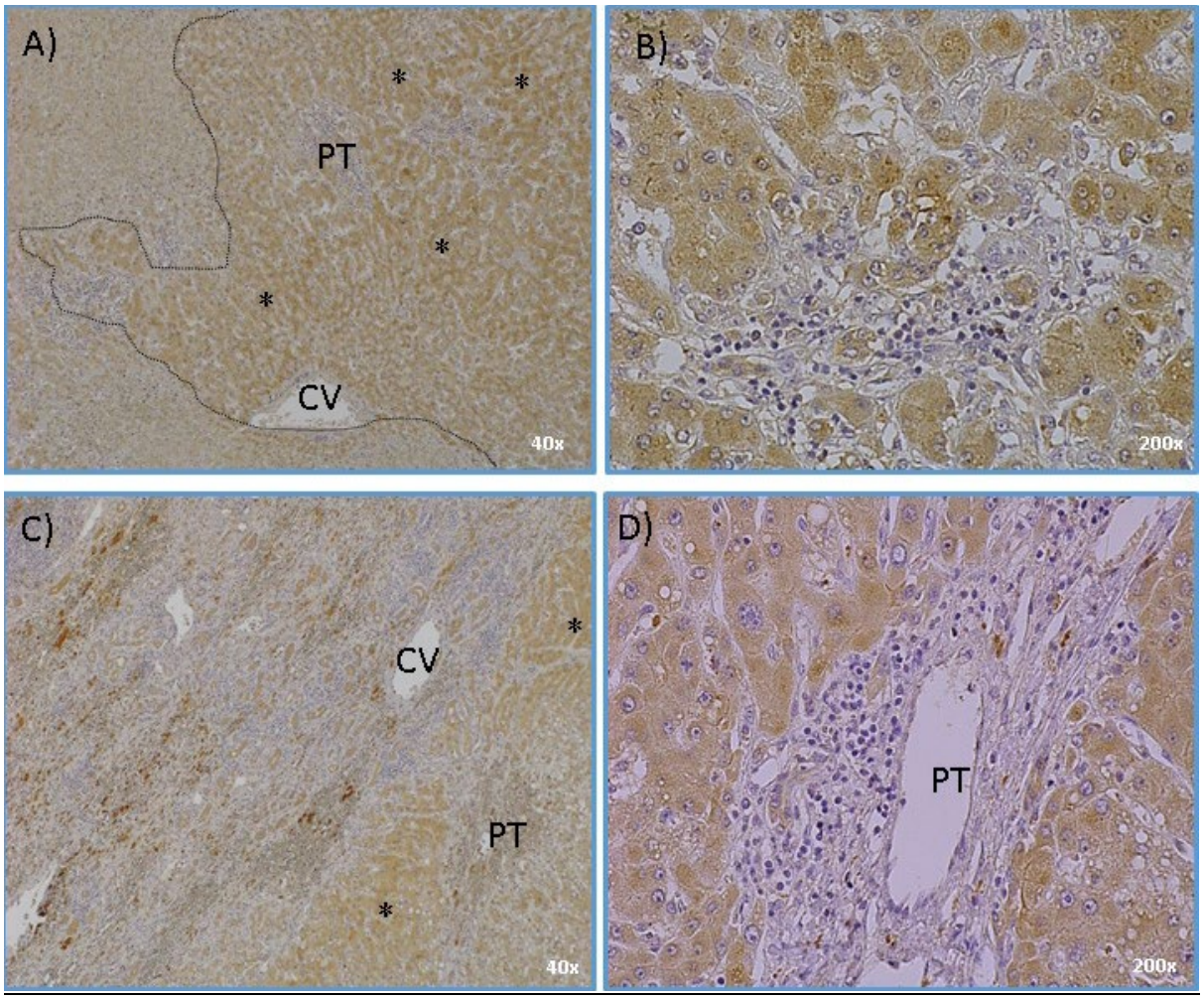

Fig. S3. Monocyte phenotypical changes in ALF

A) CCR2, HLADR and CD163 expression in fresh CD14+ cells of both ALF and HC. Results are expressed in % and MFI. Mann-Whitney test. All the comparisons are not significant, p>0.05.

B) Expression of most relevant monocyte markers according to different subsets in both acute liver failure (ALF, n=7) and healthy control (HC, n=8). 2 way ANOVA test. *p<0.05, ** p<0.01, *** p<0.001

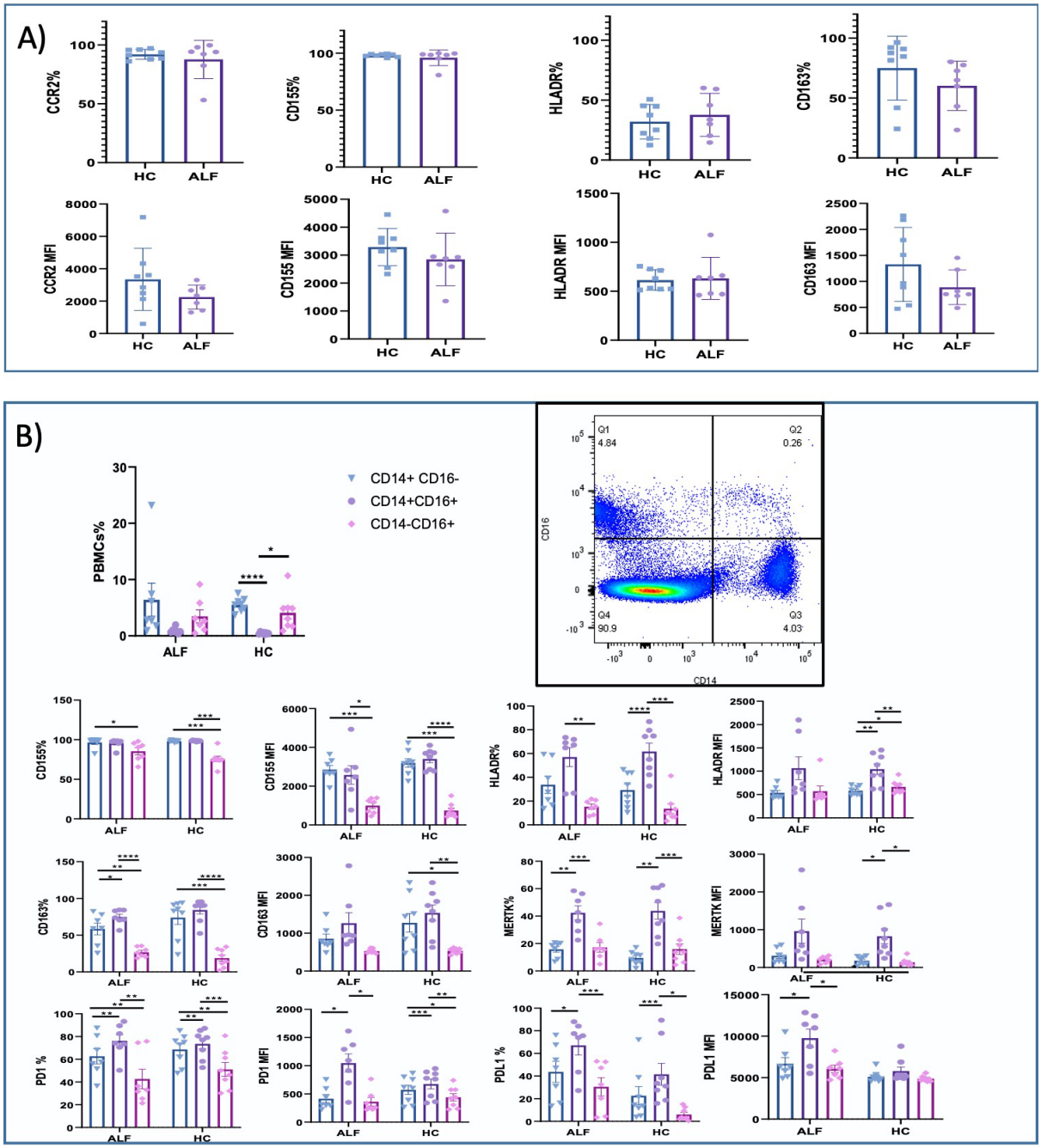

Fig. S4. NK and CD56+ T cells expression of immune check points

A) PBMCs from ALF(n=8), decompensated cirrhosis (n=7) and healthy controls (n=6) were stained for NK and CD56+T markers (CD56 and CD45) and B) we explored the expression of the markers of interest (CTLA4, PD1, PDL1, TIGIT) in these populations, Kruskal Wallis test, $p>0.05$. Although no significant, we observed on increase of CTLA 4, PD1 and PDL1 positive CD56+CD4+T cells in ALF compared to cirrhosis and healthy control. Percentage of TIGIT positive cells was increase in ALF CD56+CD8+T and NK cells compared to other groups but again this was not statistically significant, $p>0.05$

PD1: Programmed cell death 1, PDL1: Programmed cell death ligand-1, TIGIT: T cell immunoreceptor with Ig and ITIM domains, CLTA-4: Cytotoxic T-Lymphocyte Antigen 4, Tim-3: T cell immunoglobulin and mucin-domain containing-3

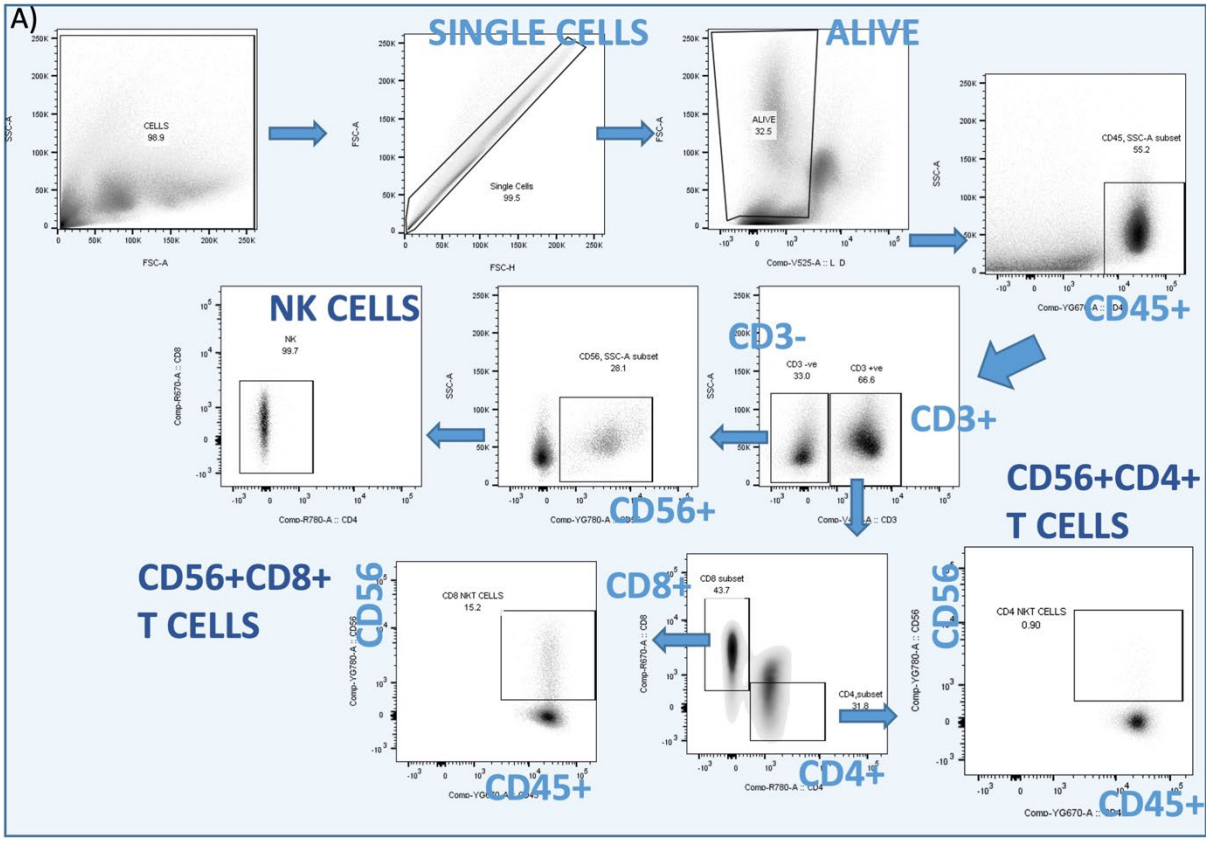
A)
SINGLE CELLS
ALIVE
CD45+
CD3-
CD3+
CD56+CD4+
T CELLS
CD4+
CD45+
CD8+
CD56+CD8+
T CELLS
CD56+
NK CELLS

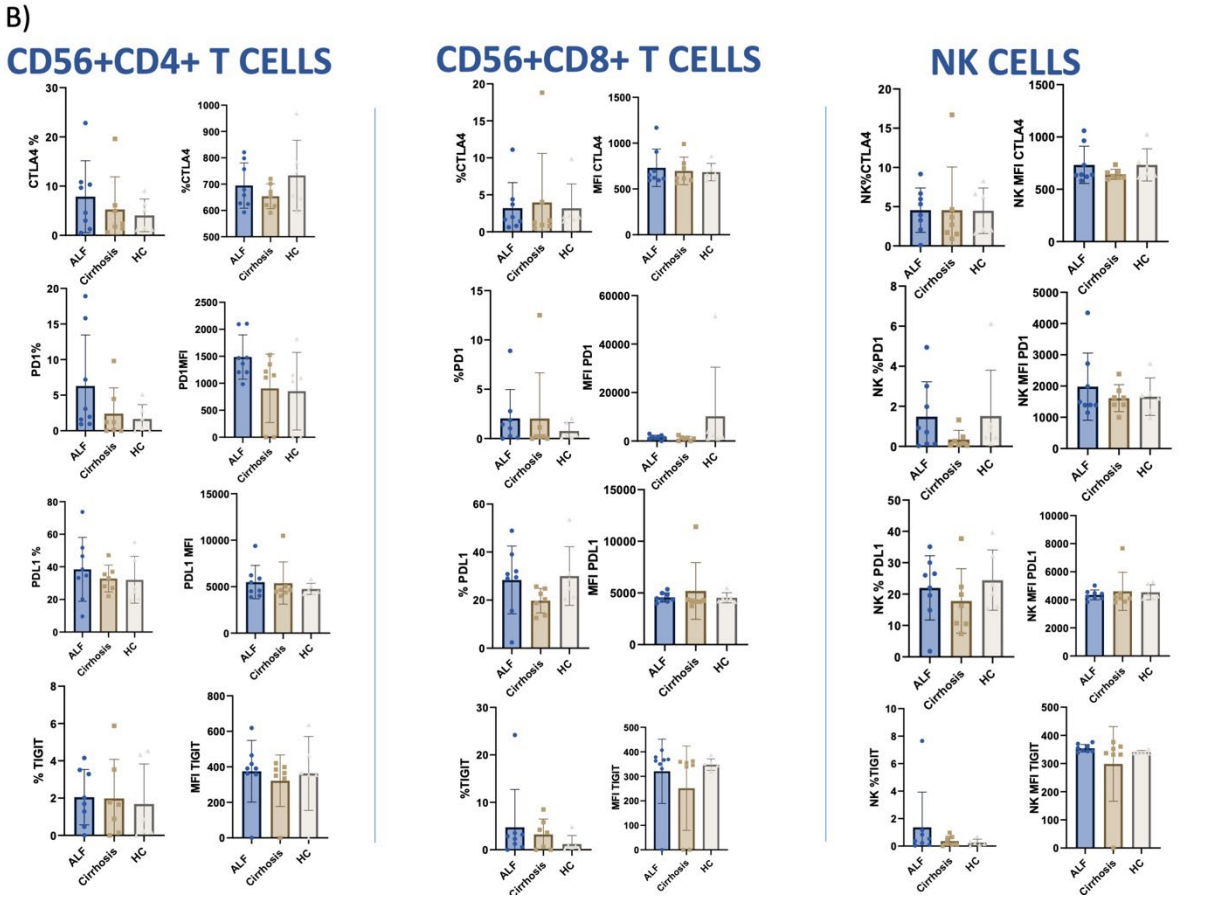
B)
CD56+CD4+ T CELLS
CD56+CD8+ T CELLS
NK CELLS
CTLA4 %
%CTLA4
MFI CTLA4
PD1%
PD1MFI
%PD1
MFI PD1
PDL1 %
PDL1 MFI
% PDL1
MFI PDL1
% TIGIT
MFI TIGIT
%TIGIT
MFI TIGIT
NK%CTLA4
NK MFI CTLA4
NK %PD1
NK MFI PD1
NK % PDL1
NK MFI PDL1
NK %TIGIT
NK MFI TIGIT
ALF
Cirrhosis
HC

Fig. S5. LPA is one of the metabolites determining phenotypical changes in ALF monocytes
PBMCs 24h culture with lipids: LPA 16:0, LPA 18:0, LPA 18:1.
HC n=4. ALF n=5, 2 way ANOVA test, *p<0.05, ** p<0.01, *** p<0.001
LPA 16:0 modulated PDL1, MerTK and CD155 expressions. PDL1 expression was increased while MerTK and CD155 reduced, compared to untreated cells. No evidence was found in T cells immune checkpoints modulation.
MerTk: Mer tyrosine kinase, PD1: Programmed cell death 1, PDL1: Programmed cell death ligand-1, TIGIT: T cell immunoreceptor with Ig and ITIM domains, CLTA-4: Cytotoxic T-Lymphocyte Antigen 4, Tim-3: T cell immunoglobulin and mucin-domain containing-3

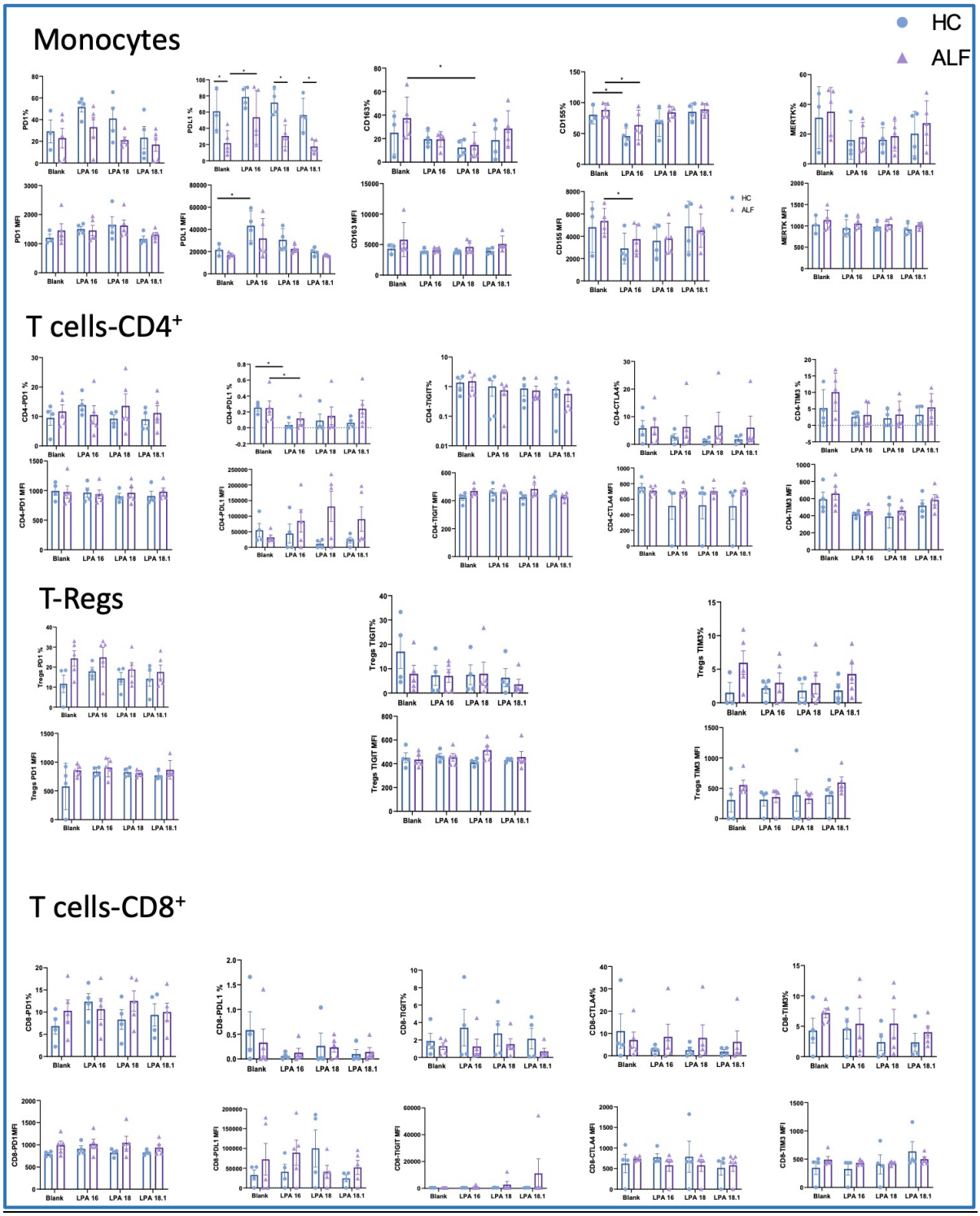

Fig. S6. Monocytes expression of LPARs in publicly available microarray data sets show a principal role of LPAR 1 and 3

A) LPAR1,3 and 6 are increased in M1 monocytes (GSE61298): Human monocyte-derived macrophages were differentiated with either granulocyte-macrophage colony-stimulating factor (GM-CSF) or macrophage colony-stimulating factor (M-CSF) and stimulated with LPS plus interferon-γ to induce macrophage polarization towards the M1 type or IL-4 to induce macrophage polarization towards the M2a type. Additionally, IL-10 was used to drive M-CSF-primed macrophages into the M2c state. Kruskal Wallis Test, *p<0.05, ** p<0.01, *** p<0.001
B) LPARs have difference expression according to monocyte subsets. Transcriptional profiling of CD16+ and CD16- peripheral blood monocytes from healthy individuals (GSE16836) revealed an increase expression of LPAR1 and 6 in CD16 negative monocytes and reduced LPAR 3 in the same population. Kruskal Wallis Test, *p<0.05, ** p<0.01, *** p<0.001
C) LPARs monocyte expression is similar in patients with paracetamol induced acute liver failure with both good and poor prognosis (GSE80751)
Kruskal Wallis Test, p>0.05

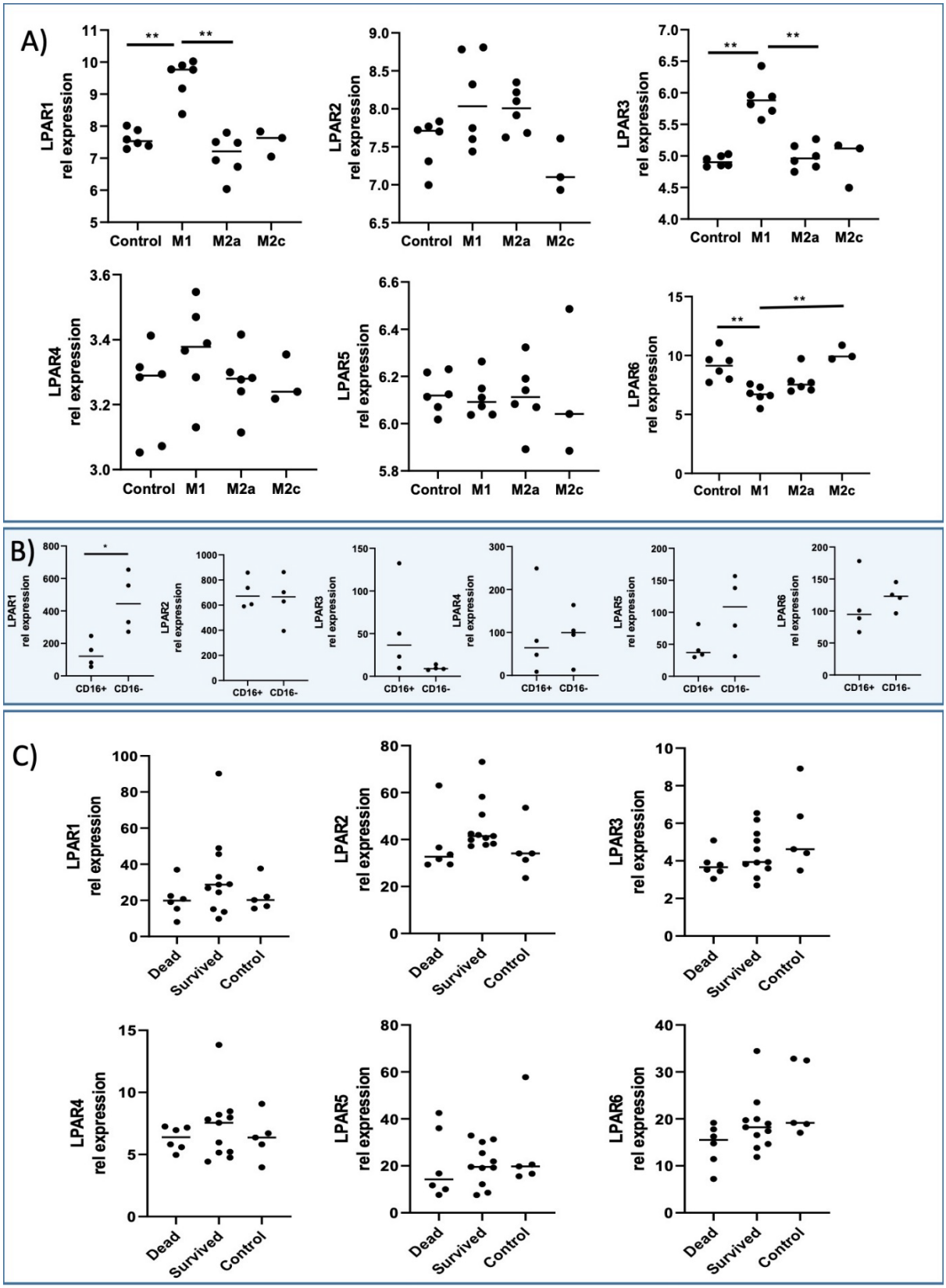
A)
LPAR1 rel expression
LPAR2 rel expression
LPAR3 rel expression
LPAR4 rel expression
LPAR5 rel expression
LPAR6 rel expression
Control M1 M2a M2c
B)
CD16+ CD16-
C)
Dead Survived Control

Fig. S7. LPAR 1 and 3 are key regulators of monocyte phenotype
Culture with LPA plus LPAR antagonist **H2L518630**, **Ro 6842262**or **Ki 16425.** LPAR 1 and 3 seem involved in monocyte modulation. Comparing to stimulation with LPA 16:0 only, the LPAR 1and 1/3 antagonist modulate the expression of several monocyte markers. Thus further experiments were focused on LPAR1 and 3 antagonism. 2 way ANOVA, *p<0.05, ** p<0.01, *** p<0.001

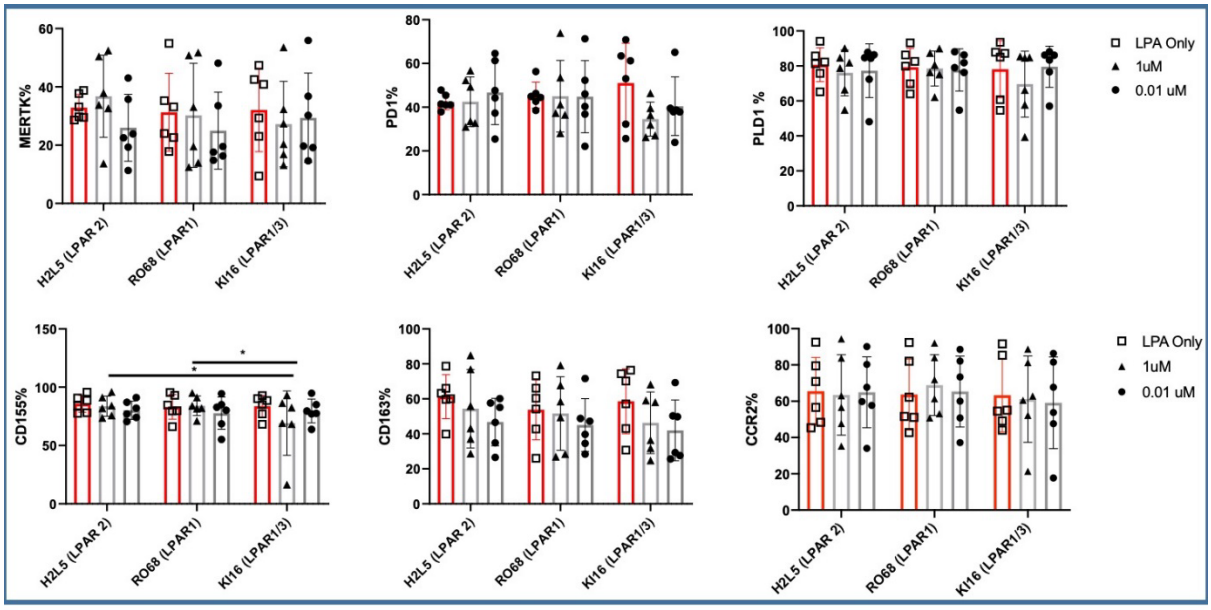

Fig. S8. Ingenuity pathway analysis (QIAGEN IPA) showing the known link between LPARs and Monocyte related genes and cytokines in acute liver failure.

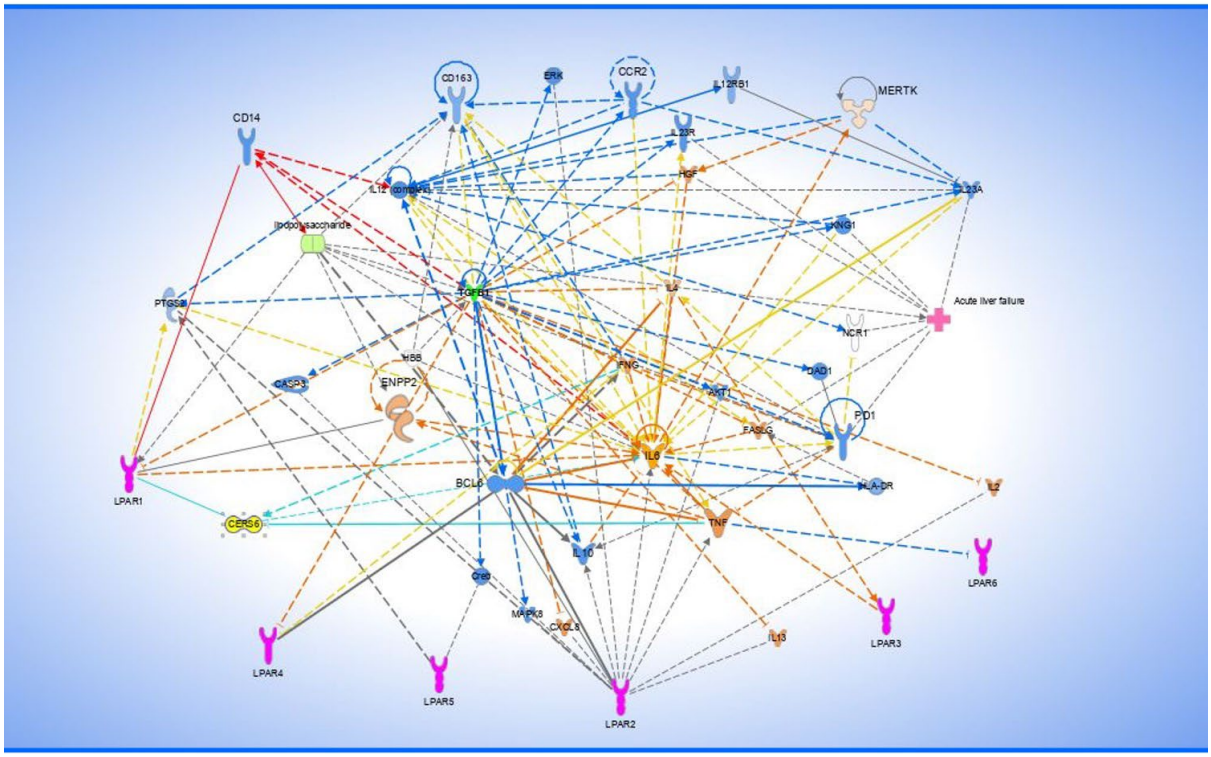

Supplementary tables

Table S1. Characteristics of the exploratory cohort used for metabolomics

	Cirrhosis		Acute Liver Disease		HC	p-value
	SC	AD	ALI	ALF		
	n=13	n=50	n=7	n=27	n=39	
Age	60 (36-80)	56 (23-73)	35 (32-51)	42 (19-59)	36 (24-69)	<0.0001
Sex (M:F)	9:4	28:22	3:4	6:21	19:19 n=38	0.006
Aetiology (Cirrhosis)						
Alcohol	7	29	N.A.	N.A.	-	0.8416
Autoimmune	2	10	N.A.	N.A.	-	
NASH	3	5	N.A.	N.A.	-	
Other	1	6	N.A.	N.A.	-	
Aetiology (ALF)						
Paracetamol	N.A.	N.A.	4	12	-	0.549
Non Paracetamol	N.A.	N.A.	3	15	-	
Child Pugh	6 (5-7)	9 (6-13)	N.A.	N.A.	-	<0.0001
MELD	9 (7-13)	12 (4-28)	42 (23-55) n=5	42 (23-55)	-	<0.0001
UKELD	49 (42-53)	55 (45-67)	N.A.	N.A.	-	<0.0001
CLIF-SOFA	4 (2-8)	7 (3-15)	8 (5-12) n=5	15 (8-20)	-	<0.0001
SOFA	4 (1-7)	5 (2-17)	6 (3-16) n=5	12 (5-18)	-	<0.0001
GCS	15 (15-15)	15 (3-15)	15 (3-15)	3 (3-15)	-	<0.0001
HE grade	0 (0-0)	0 (0-2)	0 (0-4) n=6	3 (0-4)	-	<0.0001
Hb g/dL	133 (86-159)	110 (72-162)	111 (83-143) n=6	96 (7.4-154)	-	<0.0001
INR	1.1 (1.0-1.6)	1.5 (1.1-2.9)	9.3 (1.1-15) n=6	5.8 (1.4-16.2)	-	<0.0001
WBC 10^9/L	4.5 (2.2-11.0)	6.2 (2.0-21.0)	8.3 (4.2-21.8)	11.3 (2.7-37.7)	-	<0.0001
Neutrophils 10^9/L	2.8 (1.2-7.2)	3.9 (1.1-18:0)	7.7 (2.4-20.7)	9.6 (0.4-27.5)	-	<0.0001
Lymphocytes 10^9/L	1.2 (0.6-3.4)	1.2 (0.37-3.1)	0.5 (0.3-1.9)	0.8 (0.2-0.6.8)	-	0.0265
Monocytes 10^9/L	0.4 (0.1-0.8)	0.4 (0.1-1.5)	0.4 (0.04-0.7)	0.3 (0.1-1.5)	-	0.0007
Cj Bilirubin µmol/L	7 (2-11) n=12	25 (5-447) n=41	64 (40-229) n=5	75 (13-864) n=24	-	<0.0001
Bilirubin µmol/L	19 (5-75)	52 (10-466)	70 (15-274) n=6	96 (29-1010)	-	<0.0001
IFN-γ	21.31 (4.68-577.70)	15.62 (0.08-108.7) n=47	52.55 (1.67-251.20) n=5	20.39 (0.20-1315) n=24	14.99 (4.70-145.30)	0.08
IL-10	0.52 (0.17-13.71)	0.85 (0.18-490.30) n=47	26.41 (0.36-62.79) n=5	22.26 (1.53-477.3) n=24	0.25 (0.03-14.67	<0.0001
IL-12p70	2.30 (0.26-9.22)	2.30 (0.12-176.70) n=47	1.46 (0.41-158.1) n=5	1.14 (0.10-223.8)	2.30 (0.05-2.3)	0.2259
IL-13	1.8 (1.8-34.73)	6.78 (1.8-177.6) n=47	5.38 (1.80-117.50) n=5	9.38 (1.80-84.75) n=24	1.8 (1.8-19.16)	0.0199
IL-1β	0.18 (0.16-0.68)	0.27 (0.07-122.6) n=47	0.18 (0.10-112.3) n=5	0.32 (0.11-14.65)	0.18 (0.15-1.27)	0.0005
IL-2	0.67 (0.63-1.04)	0.83 (0.21-38.21) n=47	6.11 (1.17-14.4) n=5	3.52 (0.21-14.54) n=24	0.67 (0.67-1.13)	<0.0001
IL-4	0.34 (0.05-1.40)	0.18 (0.01-0.98) n=47	0.26 (0.18-0.433) n=5	0.34 (0.02-1.08) n=24	0.17 (0.02-0.34)	0.2632
IL-6	3.61 (1.32-17.29)	8.06 (0.92-60.64) n=47	56.78 (4.21-87.68) n=5	65.93 (4.71-5745) n=24	0.84 (0.13-2.27)	<0.0001
IL-8	20.28 (9.06-437.3)	31.18 (0.05-864.3) †† n=47	383.20 (0.76-934.5) n=5	219.8 (0.18-3239) n=24	7.65 (2.65-13.73)	<0.0001

TNF-α	3.90 (2.57-11.28)	3.95 (0.48-11.95) n=47	6.92 (6.33-17.44) n=5	5.33 (0.76-21.75) n=24	1.56 (0.68-3.30)	<0.0001
Mortality % (n)						
28 day	-	-	14%(1)	33%(9)	-	-
90 day	-	-	14%(1)	44%(12)	-	-
1 year	-	-	40%(3)	48%(13)	-	-
of which Transplanted (n=)	-	-	0%	11% (3)	-	-

Table S2. Characteristics of the validation cohort used for the metabolomics study

Group	Healthy Controls n= 23	Cirrhosis n= 21	Acute liver Failure n= 43	Sepsis n= 31	p
Age, y	31 ± 8	57.5 ± 12.2	37.7 ± 15.4	62.5 ± 12.2	**<0.001**
Female, n (%)	16 (66.7)	10(47.6)	26 (60.5)	9(29)	
INR		1.5 ± 0.3	4.6 ± 4.3	1.2 ± 0.3	**<0.001**
Mortality 28, n (%)		2 (9.5%)	19(44.2%)	1(3.2%)	**<0.001**
Mortality 90, n (%)		4(19%)	19(44.2%)	1(3.3%)	**<0.001**
Albumin		32.6 ± 3.5	27 ± 5.3	29 ± 6.7	**0.006**
Bilirubin, mg/dl		2.19 ± 1.8	8.8 ± 9.9	1.7 ±4.1	**<0.001**
Haemoglobin		95.9 ± 25.6	94.6 ± 36.3	97.3 ± 28.4	0.95
White cell count		4..6 ± 2	9.3 ± 4.5	12.5 ± 7.4	**<0.001**
Neutrophils		2.7 ± 1.2	7.5 ± 4.6	13.3 ± 10.9	**<0.001**
Lymphocytes		1.2 ± 0.77	1.2 ± 2.2	5.4 ± 9.9	**0.008**
Monocytes		0.42 ± 0.22	0.66 ± 0.6	0.7 ± 0.4	0.065
CRP		12 ± 12	34.5 ± 54.9	196.9 ± 110.4	**<0.001**
MELD	6	15.9 ± 5	35.5 ± 12.2		**<0.001**
SOFA	0	2.7 ± 1.7	9.44 ± 5.3	5.2 ± 4.4	**<0.001**
RRT, n (%)		1(4.8%)	27(62%)	8(25.8%)	**<0.001**
Vasopressors, n (%)		0%	21(49%)	16(51.6%)	**<0.001**
Mech Ventilation, n (%)		0%	24(55.8%)	12(38.7%)	**<0.001**
Fio2>35%, n (%)		0%	9(21%)	12(38.7%)	**<0.001**
LysoPC 16:0	73.8 ± 26.1	50 ± 13	12.7 ± 13.3	19.2 ± 14.3	**<0.001**
LysoPC 18:0	21.6 ± 10.3	15.1 ± 3.9	3 ± 3.2	4.2 ± 3.6	**<0.001**
LysoPC 18:1	15.9 ± 7.9	15.8 ± 5	4.5 ± 4.1	4.9 ± 4.6	**<0.001**

Table S3. Antibodies used for flow cytometry.

Primary antibodies	**Host**	**Anti**	**Clone**	**Conjugated fluorophore**	**Catalogue number**	**Producer**	**Application**
CD14	Mouse	Human	M5E2	PeCy7	557742	BD	Flowcytometry
CD16	Mouse	Human	3G8	APC-H7	560195	BD	Flowcytometry
CD163	Mouse	Human	GHI/61	PE	556018	Invitrogen	Flowcytometry
CCR2	Mouse	Human	K03602	AlexaFluor 488	357226	Biolegend	Flowcytometry
HLA-DR	Mouse	Human	LN3	PerCp-Cy 5.5	45-9956-42	Invitrogen	Flowcytometry
MerTK	Mouse	Human	125518	APC	FAB8912A	R&D System	Flowcytometry
CD155	Mouse	Human	SKII.4	BV421	337632	Biolegend	Flowcytometry
PD-L1	Mouse	Human	29E.2A3	BV 605	329724	Biolegend	Flowcytometry
PD-1	Mouse	Human	EH12.1	BV786	563789	BD	Flowcytometry
CD3	Mouse	Human	SK7	eFluor 450	48-0036-42	eBioscience	Flowcytometry
Tim-3	Mouse	Human	F38-2E2	BV711	345024	Biolegend	Flowcytometry
TIGIT	Mouse	Human	MBSA43	FITC	11-9500-42	eBioscience	Flowcytometry
CTLA-4	Mouse	Human	14D3	PE	12-1529-42	eBioscience	Flowcytometry
CD25	Mouse	Human	M-A251	PE-CF594	562403	BD	Flowcytometry
CD127	Mouse	Human	eBioRDR5	PE-Cy7	25-1278-42	Invitrogen	Flowcytometry
CD8	Mouse	Human	RPA-T8	APC	17-0088-42	Invitrogen	Flowcytometry
CD4	Mouse	Human	SK3	APC-Cy7	344616	Biolegend	Flowcytometry
CD45	Mouse	Human	HI30	PE/Cy5	304009	Biolegend	Flowcytometry
CD56	Mouse	Human	QA18A21	PE/Cy7	398808	Biolegend	Flowcytometry
ATX	Mouse	Human	1F8	-	ab77104	abcam	Immunohistochemistry

Table S4. Discriminant features subjected to tandem mass spectrometry
Features that were identified from fragmentation data are highlighted in green.

Retention Time (mins)	m/z	Putative ID	Adduct
0.69	450.2	no ID match	
0.73	457.334	LPA(18:0)	[M+CH3OH+H]+
0.74	512.334	LysoPC(16:1)	[M+H+H2O]+
0.76	589.328	PA(12:0/13:0)	[M+K]+
0.78	576.361	no ID match	
1.07	540.365	LysoPC(18:1)	[M+H-H2O]+
1.30	341.186	EPA	[M+K]+
1.30	626.308	Leukotriene C4	[M+H]+
1.38	468.308	LysoPC(14:0)	[M+H]+
1.52	512.335	LysoPC(16:1)	[M+H+H2O]+
1.89	991.674	Thyroxine glucuronide	[M+K]+
4.61	328.257	no ID match	
4.61	494.354	no ID match	
4.61	495.357	no ID match	
4.61	509.325	Bassic acid	[M+Na]+
4.62	488.395	2,3-bis(Acetyloxy)propyl icosanoate	[M+NH4]+
5.35	355.284	MG(18:2)	[M+H]+
5.36	327.253	no ID match	
5.36	328.257	Clavepictine B	[M+Na]+
5.36	522.385	no ID match	
5.36	523.387	no ID match	
5.36	537.356	PA(12:0/12:0)	[M+H]+
5.37	523.382	LysoPC(P-18:1)	[M+NH4]+
6.08	355.284	MG(18:2)	[M+H]+
6.08	545.461	DG(14:0/18:3)	[M+H-H2O]+
6.18	599.505	DG(18:2/18:2)	[M+H-H2O]+
6.18	740.524	PE(16:0/20:4)	[M+H]+
6.18	741.528	no ID match	
6.18	742.528	PE(18:1/18:2)	[M+H]+
6.19	716.526	PE(16:0/18:2)	[M+H]+
6.19	718.531	PE(16:0/18:1)	[M+H]+

..

Table S5. High intensity features subjected to tandem mass spectrometry
Features that were identified from fragmentation data are highlighted in green.

Retention Time (mins)	m/z	Putative ID	Adduct
0.40	235.223	myristic acid	[M+Li]+
0.88	415.211	no ID match	
0.88	473.263	Chenodeoxycholic acid 3-sulfate	[M+H]+
1.30	585.269	Bilirubin	[M+H]+
1.30	299.138	no ID match	
1.53	433.232	LPA(16:0)	[M+Na]+
1.68	520.340	LysoPC(18:2)	[M+H]+
1.76	544.339	LysoPC(20:4)	[M+H]+
1.89	496.341	LysoPC(16:0)	[M+H]+
2.13	522.356	LysoPC(18:1)	[M+H]+
2.42	524.372	LysoPC(18:0)	[M+H]+
3.13	594.413	LysoPC(22:2)	[M+H+H2O]+
3.17	354.409	1-Tetracosene	[M+NH4]+

3.26	430.380	no ID match	
3.41	410.472	no ID match	
3.65	413.266	Nutriacholic acid	[M+Na]+
3.80	385.245	no ID match	
4.70	396.352	N-oleoyl isoleucine	[M+H]+
4.75	509.325	polyphenol-type compound	[M+Na]+
4.75	488.395	2,3-bis(Acetyloxy)propyl icosanoate	[M+NH4]+
4.77	327.253	HETE	[M+Li]+
4.96	523.472	DG(14:0/16:0)	[M+H-H2O]+
4.96	717.467	no ID match	
5.20	675.543	SM(d18:1/14:0)	[M+H]+
5.33	701.559	SM(d16:1/18:1)	[M+H]+
5.53	516.426	no ID match	
5.53	730.538	PC(16:1/16:1)	[M+H]+
5.76	780.555	PC(16:0/20:5)	[M+H]+
5.76	756.554	PC(16:0/18:3)	[M+H]+
5.92	703.575	SM(d18:1/16:0)	[M+H]+
5.92	782.569	PC(18:2/18:2)	[M+H]+
6.05	806.570	PC(16:0/22:6)	[M+H]+
6.09	732.553	PC(16:0/16:1)	[M+H]+
6.24	758.575	PC(16:0/18:2)	[M+H]+
6.24	808.584	PC(18:1/20:4)	[M+H]+
6.30	740.524	PE(16:0/20:4)	[M+H]+
6.38	784.585	PC(16:0/20:3)	[M+H]+
6.38	740.522	PE(18:2/18:2)	[M+H]+
6.45	784.585	PC(16:0/20:3)	[M+H]+
6.45	806.566	PC(18:1/20:5)	[M+H]+
6.60	734.569	PC(14:0/18:0)	[M+H]+
6.60	742.574	PC(P-16:0/18:2)	[M+H]+
6.76	794.605	PC(P-18:1/20:3)	[M+H]+
6.76	760.589	PC(16:0/18:1)	[M+H]+
6.93	810.599	PC(18:2/20:4)	[M+H]+
6.93	786.602	PC(18:0/18:2)	[M+H]+
7.12	746.604	PC(O-18:1/16:0)	[M+H]+
7.12	812.616	PC(18:0/20:3)	[M+H]+
7.42	785.652	SM(d16:1/24:1)	[M+H]+
7.42	788.615	PC(18:0/18:1)	[M+H]+
7.50	811.667	SM(d18:2/24:1)	[M+H]+
7.50	785.653	SM(d18:1/22:1)	[M+H]+
7.98	813.683	SM(d18:1/24:1)	[M+H]+
8.60	815.700	SM(d18:1/24:0)	[M+H]+
9.91	894.755	TG(18:2/18:2/18:3)	[M+NH4]+
9.91	721.507	PG(16:0/16:1)	[M+H]+
10.12	844.739	SM(d18:1/26:0)	[M+H]+
10.19	896.771	TG(18:1/18:2/18:3)	[M+NH4]+
10.19	870.755	TG(16:0/18:2/18:3)	[M+NH4]+
10.36	820.738	TG(16:0/16:1/16:1)	[M+NH4]+
10.40	846.753	TG(16:1/18:1/16:1)	[M+NH4]+
10.44	872.772	TG(16:0/18:2/18:2)	[M+NH4]+
10.67	848.770	TG(16:1/16:0/18:1)	[M+NH4]+
10.67	874.787	TG(16:0/18:1/18:2)	[M+NH4]+
10.73	900.802	TG(16:0/18:1/20:3)	[M+NH4]+
10.83	862.785	TG(16:0/17:1/18:1)	[M+NH4]+
10.96	876.803	TG(16:0/18:0/18:2)	[M+NH4]+
10.99	902.817	TG(18:1/18:1/18:1)	[M+NH4]+
11.15	852.801	TG(16:0/16:0/18:1)	[M+NH4]+
11.23	904.832	TG(18:0/18:1/18:1)	[M+NH4]+

Supplementary references

1. Beckonert O, Keun HC, Ebbels TM, et al. Metabolic profiling, metabolomic and metabonomic procedures for NMR spectroscopy of urine, plasma, serum and tissue extracts. *Nat Protoc* 2007; **2**(11): 2692-703.
2. Cloarec O, Dumas ME, Craig A, et al. Statistical total correlation spectroscopy: an exploratory approach for latent biomarker identification from metabolic 1H NMR data sets. *Anal Chem* 2005; **77**(5): 1282-9.
3. Dona AC, Jimenez B, Schafer H, et al. Precision high-throughput proton NMR spectroscopy of human urine, serum, and plasma for large-scale metabolic phenotyping. *Anal Chem* 2014; **86**(19): 9887-94.
4. Howe KL, Achuthan P, Allen J, et al. Ensembl 2021. *Nucleic Acids Res* 2021; **49**(D1): D884-D91.
5. Dobin A, Davis CA, Schlesinger F, et al. STAR: ultrafast universal RNA-seq aligner. *Bioinformatics* 2013; **29**(1): 15-21.
6. Li B, Dewey CN. RSEM: accurate transcript quantification from RNA-Seq data with or without a reference genome. *BMC Bioinformatics* 2011; **12**: 323.
7. Ritchie ME, Phipson B, Wu D, et al. limma powers differential expression analyses for RNA-sequencing and microarray studies. *Nucleic Acids Res* 2015; **43**(7): e47.
8. Luo W, Friedman MS, Shedden K, Hankenson KD, Woolf PJ. GAGE: generally applicable gene set enrichment for pathway analysis. *BMC Bioinformatics* 2009; **10**: 161.
9. Xia J, Sinelnikov IV, Han B, Wishart DS. MetaboAnalyst 3.0--making metabolomics more meaningful. *Nucleic Acids Res* 2015; **43**(W1): W251-7.
10. Kanehisa M, Araki M, Goto S, et al. KEGG for linking genomes to life and the environment. *Nucleic Acids Res* 2008; **36**(Database issue): D480-4.